JOURNAL OF GEOPHYSICAL RESEARCH, VOL. 106, NO. B8, PAGES 16,435–16,460, AUGUST 10, 2001

Dynamics of the India-Eurasia collision zone

Lucy M. Flesch

Department of Geosciences, State University of New York at Stony Brook, Stony Brook, New York

A. John Haines

Bullard Laboratories, University of Cambridge, Cambridge, England, United Kingdom

William E. Holt

Department of Geosciences, State University of New York at Stony Brook, Stony Brook, New York

Abstract. We present simple new dynamic calculations of a vertically averaged deviatoric stress field (over a depth average of 100 km) for Asia from geodetic, geologic, topographic, and seismic data. A first estimate of the minimum absolute magnitudes and directions of vertically averaged deviatoric stress is obtained by solving force balance equations for deviatoric stresses associated with gravitational potential energy differences within the lithosphere plus a first-order contribution of deviatoric stresses associated with stress boundary conditions. This initial estimate of the vertically averaged deviatoric stress field is obtained independent of assumptions about the rheology of the lithosphere. Absolute magnitudes of vertically averaged deviatoric stresses vary between 5 and 40 MPa. Assuming bulk viscous behavior for the lithosphere, the magnitudes of deviatoric stresses, together with the magnitudes of strain rates inferred from Quaternary fault slip rate and GPS data, yield vertically averaged effective viscosities for Tibet of 0.5-5$\times 10^{22}$ Pa s, compared with 1-2.5$\times 10^{23}$ Pa s in more rigid areas elsewhere in the region. A forward modeling method that solves force balance equations using velocity boundary conditions allows us to refine our estimates of the vertically averaged effective viscosity distribution and deviatoric stress field. The total vertically averaged deviatoric stress and effective viscosity field are consistent with a weak lower crust in Tibet; they are consistent with some eastward motion of Tibet and south China lithosphere relative to Eurasia; and they confirm that gravitational potential energy differences have a profound effect on the spatially varying style and magnitude of strain rate around the Tibetan Plateau. Our results for the vertically averaged deviatoric stress argue for a large portion of the strength of the lithosphere to reside within the seismogenic upper crust to get deviatoric stress magnitudes there to be as high as 100-300 MPa (in accord with laboratory and theoretical friction experiments indicating that stress drops in earthquakes are small fractions of the total deviatoric stress).

1. Introduction

Soon after the discovery of plate tectonics it became obvious that deformation within continental regions occurs differently from that along oceanic plate boundary zones. Whereas most oceanic plate boundary zones are narrow, continental zones are several hundred to thousands of kilometers wide [*McKenzie*, 1972; *Molnar and Tapponnier*, 1975; *Molnar*, 1988] (Figure 1a). Despite universal agreement that continental regions behave as wide zones of deformation, considerable controversy remains on the behavior of continental lithosphere and the nature, magnitude, and source of the forces that affect continental deformation. With regard to the behavior of continental lithosphere, there are two primary schools of thinking. The first school regards continental lithosphere as generally plate-like in behavior, consisting of numerous relatively coherent continental blocks, separated by narrow zones of shear or deformation that penetrate through the entire lithosphere [*Tapponnier et al.*, 1982; *Peltzer and Tapponnier*, 1988; *Avouac and Tapponnier*, 1993]. Tractions applied to the boundaries, and the frictional properties of the shear zones, affect block movement and terrane displacement. The second school considers the bulk behavior of deforming continental lithosphere as continuous. Many of those who treat deformation on a lithospheric scale as continuous have performed numerical solutions [*Tapponnier and Molnar*, 1976; *Bird and Piper*, 1980; *England and McKenzie*, 1982; *Vilotte et al.*, 1982; *England and*

Paper number 2001JB000208.
0148-0227/01/2001JB000208$09.00

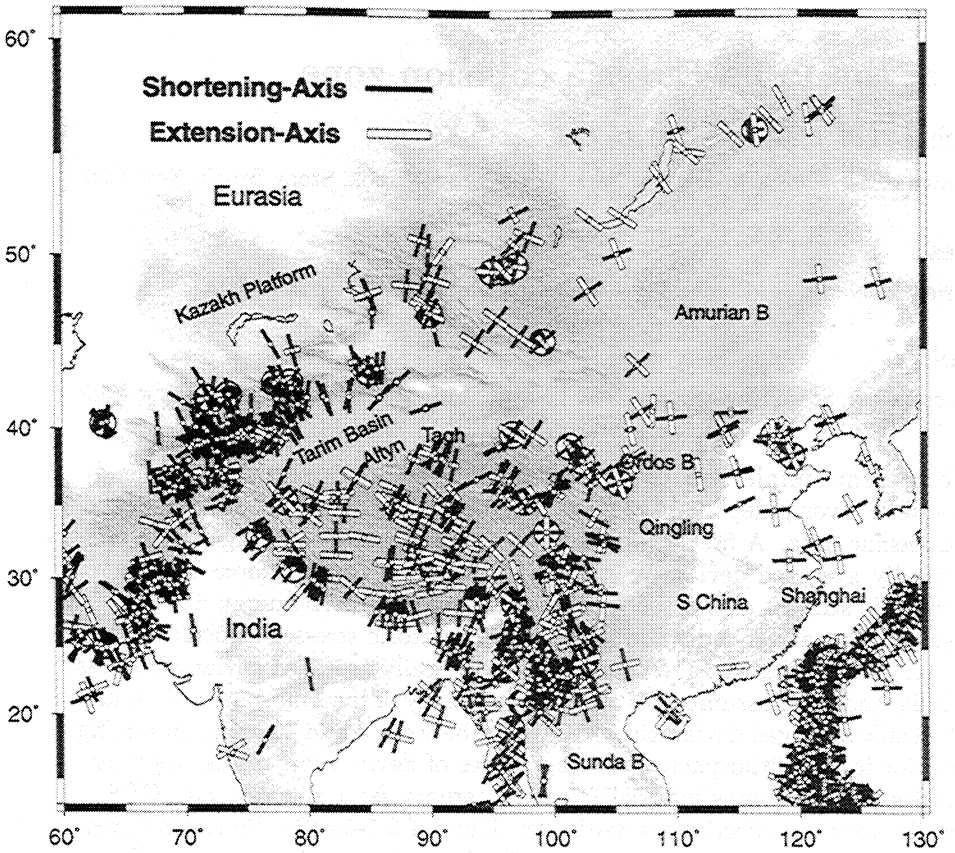

Figure 1a. Horizontal contraction (solid) and extension (open) strain axes directions associated with earthquakes larger than $\sim M_w > 5.5$ between 1963 and 1998, showing the distributed nature of the deformation around the India-Eurasia collision zone as well as the spatial variation in the strain field [*Holt et al.*, 1995]. Focal mechanisms are for large events with $M_w > 7.0$; a few large historic events (pre-1963) are also shown [*Molnar and Deng*, 1984].

Houseman, 1986; *Houseman and England*, 1993] or mechanical analog models [*Cobbold and Davy*, 1988] of a thin viscous sheet under the influence of gravity perpendicular to it. Thin viscous sheet models often involve a vertical average of rheology of the lithosphere [*Sonder and England*, 1986]. The great advantage of this model is that it includes the effects of body forces associated with crustal thickness contrasts or gravitational potential energy (GPE) differences that have an important influence on continental deformation [e.g., *Frank*, 1972; *Artyushkov*, 1973; *Dalmayrac and Molnar*, 1981; *Fleitout and Froidevaux*, 1982; *Molnar and Lyon-Caen*, 1988; *Jones et al.*, 1996].

Deformation within the India-Eurasia collision zone has received considerable attention because it constitutes the largest area of continental deformation zone in the world. Block tectonic experiments applied to Asia suggest a considerable amount of eastward displacement or extrusion of continental crustal lithosphere relative to both Eurasia and India, accommodated along narrow strike-slip shear zones [*Tapponnier et al.*, 1982; *Peltzer and Tapponnier*, 1988]. On the other hand, the thin viscous sheet calculations produce limited strike-slip deformation and eastward displacement rates of Asia crust no greater than ~1 cm/yr [*England and Houseman*, 1986; *Houseman and England*, 1993; *Molnar and Gipson*, 1996]. Elsewhere, we have determined [*Haines*, 1982; *Haines and Holt*, 1993; *Haines et al.*, 1998] a strain rate and velocity field, [*Holt et al.*, 2000a, 2000b], constrained using both Quaternary fault slip rates [*England and Molnar*, 1997a] and recent GPS measurements [*Abdrakhmatov et al.*, 1996; *Yu et al.*, 1999; *Calais et al.*, 1998; *Larson et al.*, 1999; *Heki et al.*, 1999; *Simons et al.*, 1999; *Bendick et al.*, 2000; *Chen et al.*, 2000; *Shen et al.*, 2000; *Zhu et al.*, 2000], and the International GPS Service (IGS) global velocity solution of GPS vectors, which are available on the Web (http://sideshow.jpl.nasa.gov/mbh/series.html). The IGS velocities referenced in this paper were obtained from this Web site for solution 1999.5 and are hereafter referred to as IGS. The kinematic model (Figures 1b and 1c) shows ESE displacement of crustal material relative to Eurasia of ~8-10 mm/yr at Shanghai, China, and 9-13 mm/yr ESE in southernmost China and Indo-China (Figure 1c).

The kinematics of crustal deformation within Asia are defined well enough that it is possible to refine inferences on the dynamic processes influencing the de-

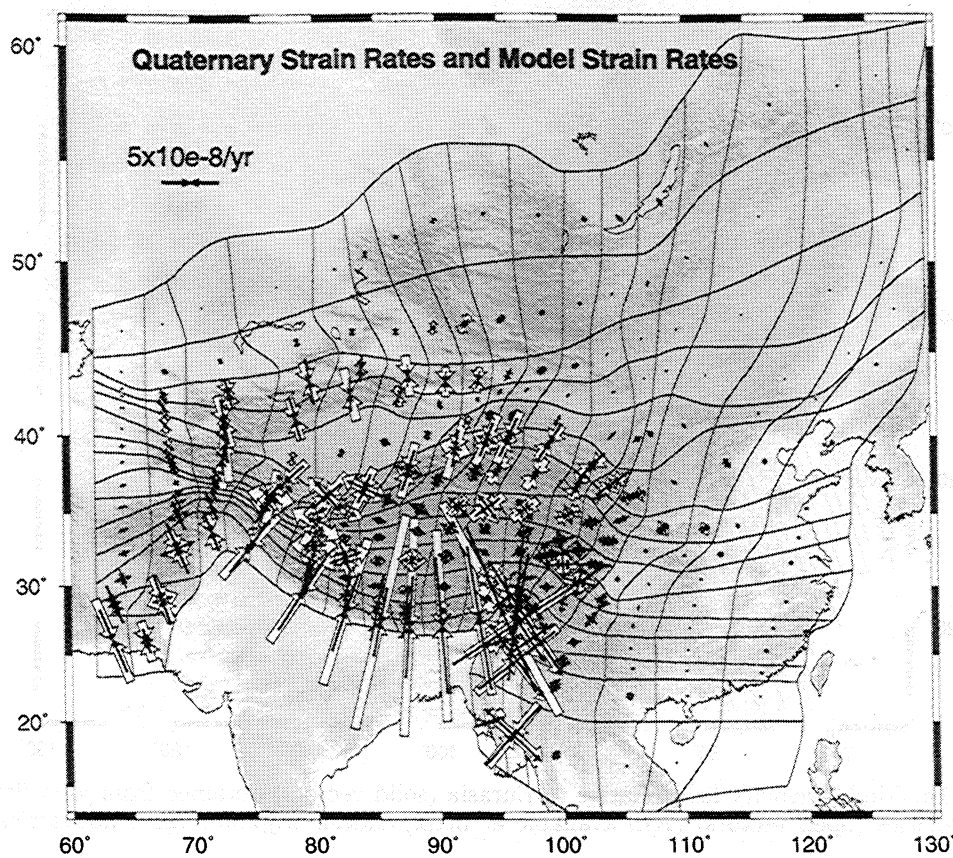

Figure 1b. Observed horizontal strain rates (open principal strain axes), inferred within areas in irregular grid using Quaternary fault slip rates [*England and Molnar*, 1997a], and model strain rates (plotted as averages within areas using solid principal strain axes) from a joint fitting of GPS velocities (IGS available at http://sideshow.jpl.nasa.gov/mbh/series.html) [*Abdrakhmatov et al.*, 1996; *Calais et al.*, 1998; *Simons et al.*, 1999; *Larson et al.*, 1999; *Heki et al.*, 1999; *Yu et al.*, 1999; *Bendick et al.*, 2000; *Chen et al.*, 2000; *Shen et al.*, 2000; *Zhu et al.*, 2000] and Quaternary fault slip rates using bicubic Bessel interpolation [*deBoor*, 1978] of velocities on a curvilinear grid [*Haines et al.*, 1998; *Holt et al.*, 2000b].

formation field. *England and Molnar* [1997b] solved for a dimensionless GPE field by integrating their strain rate data and matched it to the observed GPE to show that the dynamics of Asia can be explained in terms of a kinematic solution. This is an important result, but their method [*England and Molnar*, 1997a, 1997b] does not constrain the magnitudes of deviatoric stress or viscosity in regions other than Tibet.

In this paper we use a thin viscous sheet approach to seek a simple dynamic parameterization that can describe the present-day deformation field in Asia. The first stage of the modeling involves a new approach that enables us to directly estimate deviatoric stresses associated with GPE differences within the lithosphere (section 2). This approach enables us to separate out and solve for the intrinsic contributions of the absolute magnitudes and styles of the deviatoric stress that results from density variations within the lithosphere and then use these estimates to solve for the extrinsic stresses related to the accommodation of plate motion (section 3). This determination of absolute values of the deviatoric stress field (the sum of the two deviatoric stress field solutions from buoyancy and boundary forces) is the first step in finding a final dynamic solution (the stress field boundary conditions (section 3) are only an approximation, as is the minimum stress approach in section 2). The second step involves using kinematic strain rate data to infer estimates of the vertically averaged effective viscosity distribution of the lithosphere in Asia (section 4). The third and final step involves the solutions to the force balance equations (section 5), in which we use velocity boundary conditions from the kinematic solution, GPE variations determined in section 2, and the viscosity distribution determined in section 4 to further refine our dynamic solution.

2. Deviatoric Stresses Associated With Gravitational Potential Energy Variations

Many studies of the dynamics of continental lithosphere have shown that variations of GPE within the lithosphere have an important influence on the style and magnitude of the stresses driving deformation [e.g.,

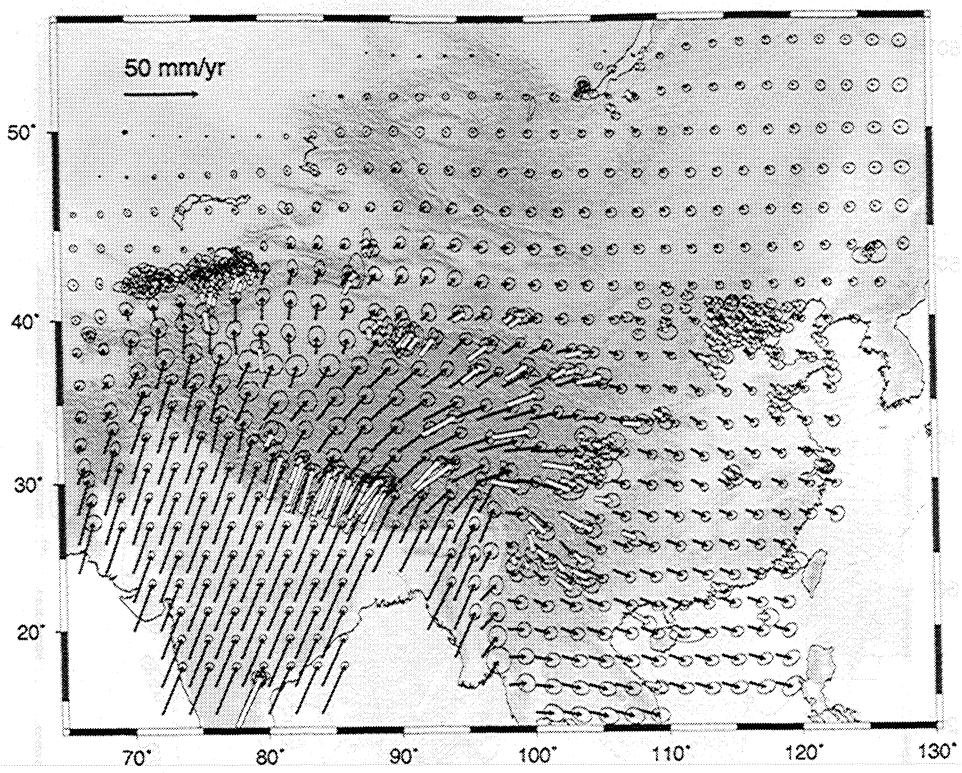

Figure 1c. Model velocity field relative to Eurasia (solid vectors) obtained from joint fitting of GPS velocities (open vectors) (IGS available at http://sideshow.jpl.nasa.gov/mbh/series.html) [*Abdrakhmatov et al.*, 1996; *Calais et al.*, 1998; *Simons et al.*, 1999; *Larson et al.*, 1999; *Heki et al.*, 1999; *Yu et al.*, 1999; *Bendick et al.*, 2000; *Chen et al.*, 2000; *Shen et al.*, 2000; *Zhu et al.*, 2000] and Quaternary strain rates [*England and Molnar*, 1997a] with continuous, self-consistent functions (same as in solution in Figure 1b) [*Holt et al.*, 2000b]. Error ellipses for both GPS vectors and model vectors are for 95% confidence. The solutions shown in Figure 1b and 1c are slightly updated from the solution presented by *Holt et al.* [2000b]. In this solution an additional 126 GPS vectors (total of 364 vectors) were added to the data set from recent studies of *Bendick et al.* [2000], *Shen et al.* [2000], and *Chen et al.* [2000]. The addition of these vectors to the set of GPS observations that are fitted in the inversion changed the model velocity values along the boundaries of the grid by >5% everywhere. The GPS vectors (open vectors) are in a model Eurasian frame of reference, which is solved for in the inversion [*Holt et al.*, 2000b].

England and McKenzie, 1982; *England and Houseman*, 1986; *Molnar and Lyon-Caen*, 1988; *Coblentz et al.*, 1994; *Jones et al.*, 1996; *England and Molnar*, 1997b]. *Flesch et al.* [2000] have shown that it is possible to directly solve the force balance equations for an estimate of the vertically averaged deviatoric stress tensor field associated with GPE variations in the lithosphere. In this method, outlined below, no assumptions are made about the values of vertically averaged rheology. We start with the Stokes equation of steady motion, neglecting rate of change of momentum

$$\frac{\partial \sigma_{ij}}{\partial x_j} + \rho g \widehat{z}_i = 0, \tag{1}$$

where σ_{ij} is the total stress, ρ is the density, g is the gravitational acceleration, and $\widehat{z}_i$ is the unit vector in the vertical direction. Equation (1) uses summation notation, where i is given values of x, y, and z and the repeated index j is used to represent the summation over x, y, and z. In accord with other studies that have addressed the behavior of a thin viscous sheet [e.g., *Bird and Piper*, 1980; *England and McKenzie*, 1982; *England and Houseman*, 1986] we integrate stresses vertically and then make a simplifying assumption: That is, first, we integrate (1) over the thickness of the sheet (such that we form vertical averages of stress), and second, we assume no tractions at the base of the sheet. Because the aspect ratio of length of thin sheet (thousands of kilometers) versus its thickness (about 100 km) is large, the first step is, to the first order, reasonable. The vertically integrated horizontal equations of motion for an isotropic, incompressible medium can thus be written

$$\frac{\partial \overline{\tau}_{xx}}{\partial x} - \frac{\partial \overline{\tau}_{zz}}{\partial x} + \frac{\partial \overline{\tau}_{xy}}{\partial y} + \frac{\partial \overline{\sigma}_{zz}}{\partial x} = 0 \tag{2a}$$

$$\frac{\partial \overline{\tau}_{xy}}{\partial x} + \frac{\partial \overline{\tau}_{yy}}{\partial y} - \frac{\partial \overline{\tau}_{zz}}{\partial y} + \frac{\partial \overline{\sigma}_{zz}}{\partial y} = 0, \tag{2b}$$

where

$$\overline{\sigma}_{zz} = -\frac{1}{\overline{h}} \int_0^h \left[\int_0^z \rho(z') g dz' \right] dz \qquad (3)$$

is the vertically averaged vertical stress of a column of lithosphere, which has units of potential energy per unit volume. The vertically averaged vertical stress, $\overline{\sigma}_{zz}$, is equivalent, though opposite in sign, to what others have referred to as gravitational potential energy (GPE), divided by an assumed average thickness of the thin sheet $\overline{h}$ [*England and McKenzie*, 1982; *England and Houseman*, 1986; *Jones et al.*, 1996; *England and Molnar*, 1997b]. Here we refer to $\overline{\sigma}_{zz}$ as GPE. In (3), $\rho(z')$ is the density, which varies with depth, and g is gravitational acceleration. The average thickness of the sheet (lithosphere), $\overline{h}$, is here taken to be 100 km and is used everywhere to convert depth integrals of stresses into depth "averages." (These expressions and those below are for the flat Earth approximation. We actually use instead the corresponding expressions for the spherical Earth, which have the same structure but less simple forms.) Equations (2a) and (2b) state that horizontal gradients of deviatoric stress within the lithosphere are balanced by horizontal gradients of GPE. Gravity anomalies indicate that over length scales of a few hundred kilometers, higher elevations are supported by roots of low density crust relative to the surrounding mantle [*England and Molnar*, 1997b; *McKenzie and Fairhead*, 1997]. Furthermore, the gravity field in Tibet indicates that the topography there is for the most part in local Airy isostatic compensation [*Jin et al.*, 1994]. Assuming local Airy isostatic compensation of topography relative to a standard mid-ocean ridge column, we infer values for $\overline{\sigma}_{zz}$ and seek solutions to (2a) and (2b).

Applying the thin sheet approximation to the force balance equation (1) leaves us with two equations (equations (2a) and (2b)) and three unknowns ($\overline{\tau}_{xx}, \overline{\tau}_{yy}, \overline{\tau}_{xy}$). We eliminate one degree of freedom by seeking the minimum root mean square deviatoric stress field, subject to the constraint that (2a) and (2b) are satisfied. To do this, we optimize the functional

$$I = \int_S \left[\overline{\tau}_{\alpha\beta} \overline{\tau}_{\alpha\beta} + (\overline{\tau}_{\gamma\gamma})^2 \right] dS$$

$$+ \int_S 2\lambda_\alpha \left[\frac{\partial}{\partial x_\beta} (\overline{\tau}_{\alpha\beta} + \delta_{\alpha\beta} \overline{\tau}_{\gamma\gamma}) + \frac{\partial \overline{\sigma}_{zz}}{\partial x_\alpha} \right] dS, \qquad (4)$$

where S is the area of the Earth's surface being considered, $\overline{\tau}_{\alpha\beta}$ is the vertically integrated horizontal deviatoric stress tensor (i.e. xx, xy, yx, and yy components), and $\overline{\tau}_{\gamma\gamma} = \overline{\tau}_{xx} + \overline{\tau}_{yy} = -\overline{\tau}_{zz}$. Optimization of (4) involves the minimization of the second invariant of the stress field (first integral), subject to the constraint that this stress field satisfies the force balance equations (equations (2a) and (2b)) (second integral), where $\Lambda = (\lambda_x, \lambda_y)$ are Lagrange multipliers for the force balance constraint. Equations (2a) and (2b) are now written in (4) using summation notation, where α represents either x or y and the repeated index β is used to represent the summation over x and y. Using the variational principle [*Morse and Feshbach*, 1953] to optimize (4) with respect to $\overline{\tau}_{\alpha\beta}$ (see Appendix A for details) yields

$$\overline{\tau}_{\alpha\beta} = \frac{1}{2} \left(\frac{\partial \lambda_\alpha}{\partial x_\beta} + \frac{\partial \lambda_\beta}{\partial x_\alpha} \right) \qquad (5)$$

at all points inside S and $\Lambda = (\lambda_x, \lambda_y) = 0$ at all points on the boundary ∂S (except anywhere on the boundary where tractions are constrained to be zero). That is, $\overline{\tau}_{\alpha\beta}$ is related to the vector of Lagrangian multipliers $\Lambda = (\lambda_x, \lambda_y)$ in the same way that strain rate $\dot{\varepsilon}_{\alpha\beta}$ is related to the velocity vector $\mathbf{v} = (u_x, u_y)$. Substituting (5) into (2a) and (2b) gives the force balance equations that the Lagrange multipliers, $\Lambda = (\lambda_x, \lambda_y)$, have to satisfy (written in summation notation):

$$\frac{\partial}{\partial x_\beta} \left[\frac{1}{2} \left(\frac{\partial \lambda_\alpha}{\partial x_\beta} + \frac{\partial \lambda_\beta}{\partial x_\alpha} \right) + \delta_{\alpha\beta} \frac{\partial \lambda_\gamma}{\partial x_\gamma} \right] = -\frac{\partial \overline{\sigma}_{zz}}{\partial x_\alpha}, \qquad (6)$$

where $\partial \lambda_\gamma / \partial x_\gamma = \partial \lambda_x / \partial x + \partial \lambda_y / \partial y$. Then, again using the variational principle, it can be shown that minimization of a functional J with respect to $\Lambda = (\lambda_x, \lambda_y)$, where

$$J = \int_S \left[2 \left(\overline{\tau}_{xx} + \frac{1}{3} \overline{\sigma}_{zz} \right)^2 + 2 \left(\overline{\tau}_{xx} + \frac{1}{3} \overline{\sigma}_{zz} \right) \right.$$

$$\left. \left(\overline{\tau}_{yy} + \frac{1}{3} \overline{\sigma}_{zz} \right) + 2 \left(\overline{\tau}_{yy} + \frac{1}{3} \overline{\sigma}_{zz} \right)^2 + 2 \overline{\tau}_{xy}^2 \right] dS \qquad (7)$$

provides a solution to (2a) and (2b) that corresponds to the minimum possible vertically averaged deviatoric stress associated with GPE differences in the lithosphere (see Appendix B for details).

Assuming Airy isostasy, we estimate the vertically averaged vertical stress, $\overline{\sigma}_{zz}$, using an average crustal density of 2828 kg/m^3, which maintains Airy isostasy for a crustal thickness of 70 km and corresponding elevation of 5 km in Tibet (with an assumed mantle density of 3300 kg/m^3). We have chosen 100 km as the average lithospheric thickness $\overline{h}$ (following *Jones et al.* [1996]) and assume that below this depth, there are no longer any significant lateral variations in density caused by topography. We then minimize (7), with respect to $\Lambda = (\lambda_x, \lambda_y)$, using a finite element approach, to determine an estimate of the vertically averaged deviatoric stress field that results from GPE differences within the lithosphere (Figure 2a). The deviatoric stress magnitudes resulting from GPE differences are of the order of 10-20 MPa, they vary rapidly spatially, and they are dominated by compressional deviatoric stresses at low elevations and extensional deviatoric stresses at high elevation (Figure 2a).

Differences in magnitude of $\overline{\sigma}_{zz}$ between Tibet and

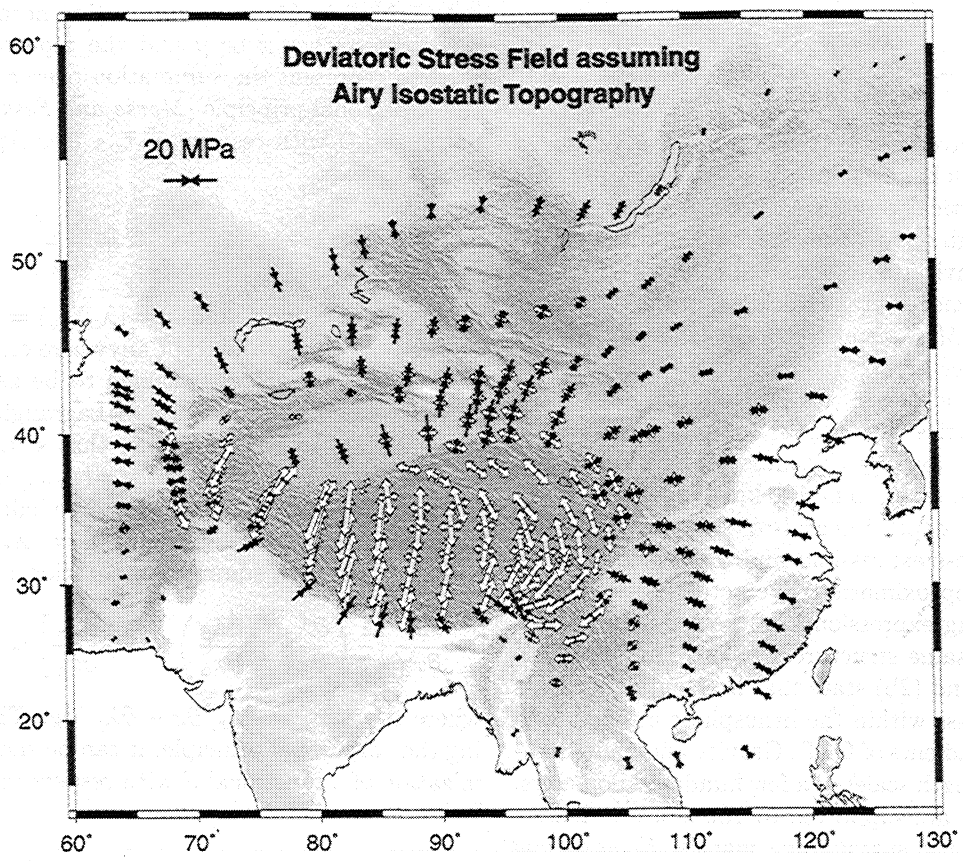

Figure 2a. The minimum root mean square deviatoric stress field that satisfies force balance equations, where sources of stress are gravitational potential energy differences (GPE) inferred assuming local Airy isostatic compensation of topography in Asia. Open principal axes represent tensional deviatoric stress. Solid axes are principal compressional deviatoric stress.

regions near sea level are $\sim 7.5 \times 10^7$ N/m^2 or $\sim 7.5 \times 10^{12}$ N/m (using the defined 100-km lithospheric thickness). This value of force per unit length is roughly equivalent to the magnitude of force per unit length proposed by *Molnar and Lyon-Caen* [1988] and *Molnar et al.* [1993] that an Airy isostatically balanced Tibetan Plateau and the surrounding low-elevation regions exert upon one another [e.g., see *Dalmaryac and Molnar*, 1981]. However, maximum stress differences between high-elevation regions and low-elevation regions in our model (Figure 2a) are only $\sim 3.2 \times 10^7$ N/m^2 ($\sim 3.2 \times 10^{12}$ N/m), which is only half of the difference in force per unit length between the Tibetan Plateau and regions near sea level proposed by *Molnar et al.* [1993]. These predicted differences in force per unit length can be related to the force balance equations that we are solving, which include terms involving $\overline{\tau}_{xx} + \overline{\tau}_{yy} = -\overline{\tau}_{zz}$ in conjunction with the $\partial \overline{\tau}_{zz}/\partial x$ and $\partial \overline{\tau}_{zz}/\partial y$ terms in (2a) and(2b). However, replacing $\overline{\tau}_{xx} - \overline{\tau}_{zz}$ with $\overline{\tau}_{xx}$ and $\overline{\tau}_{yy} - \overline{\tau}_{zz}$ with $\overline{\tau}_{yy}$, in the fashion of *Dalmayrac and Molnar* [1981] and *Molnar and Lyon-Caen* [1988], in effect replaces the constraint $\overline{\tau}_{xx} + \overline{\tau}_{yy} + \overline{\tau}_{zz} = 0$ with an alternative definition of deviatoric stress based on $\overline{\tau}_{zz} = 0$ (alternatively, one could set either $\overline{\tau}_{xx} = 0$ or $\overline{\tau}_{yy} = 0$). A consequence of defining deviatoric stress using the "three-dimensional" constraint $\overline{\tau}_{xx} + \overline{\tau}_{yy} + \overline{\tau}_{zz} = 0$, as we have done (and is also done by *England and Molnar* [1997b]), is that horizontal stress magnitudes should be about half of those predicted by a "two-dimensional" treatment based on $\overline{\tau}_{zz} = 0$ [e.g., *Dalmayrac and Molnar*, 1981; *Molnar and Lyon-Caen*, 1988; *Molnar et al.*, 1993], since in the three-dimensional treatment the remainder of the differences in $\overline{\sigma}_{zz}$ values are absorbed in the vertical deviatoric stress $\overline{\tau}_{zz}$.

We have varied grid geometry and experimented with different average crustal densities and found that the pattern of deviatoric stress was relatively insensitive to both. Extending the grid into India introduced compressional deviatoric stress in the Indian plate but did not change the current pattern of deviatoric stress distribution in the interior of the grid (Figure 2a). Extending the boundaries of the grid into the northern Eurasian plate also introduced compressional deviatoric stress into this stable region and decreased compressional deviatoric stresses in south China by ~10%. The deviatoric stress in Tibet and the Tien Shan did not change. Grid boundaries only have a significant effect on the style of deviatoric stress if the boundary crosses into a region of high GPE from a region of low topography. In this case, large compressional deviatoric stresses

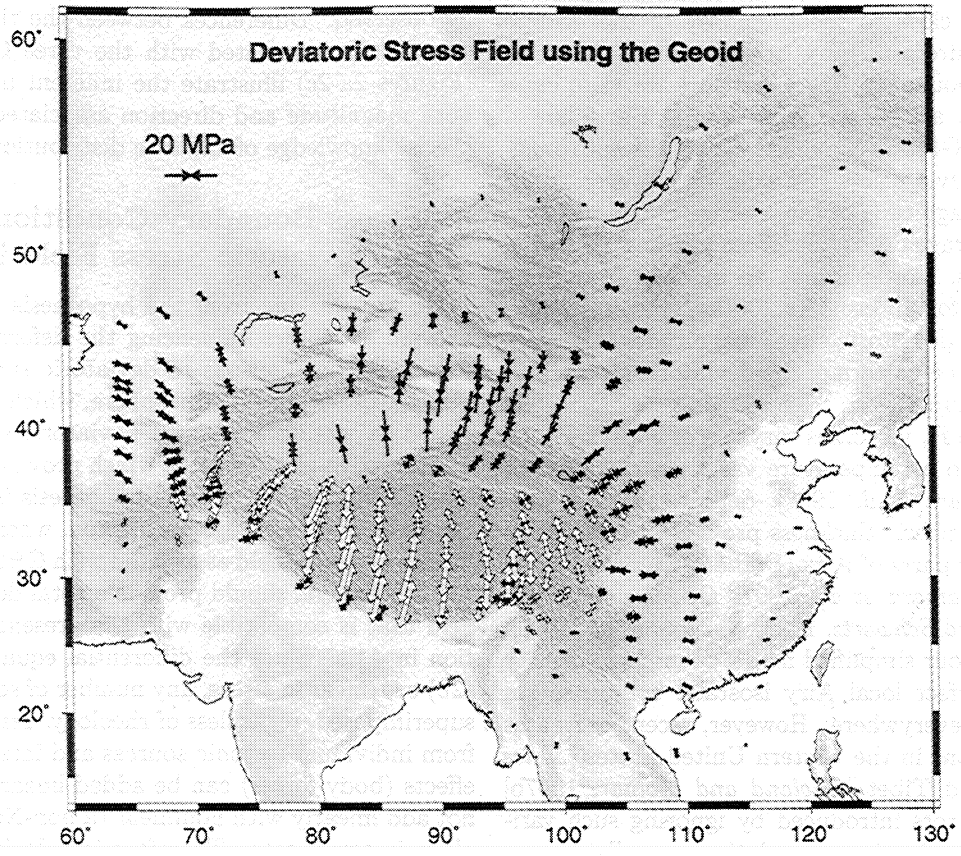

Figure 2b. Same as Figure 2a only GPE estimates were inferred from the EGM 96 geoid model.

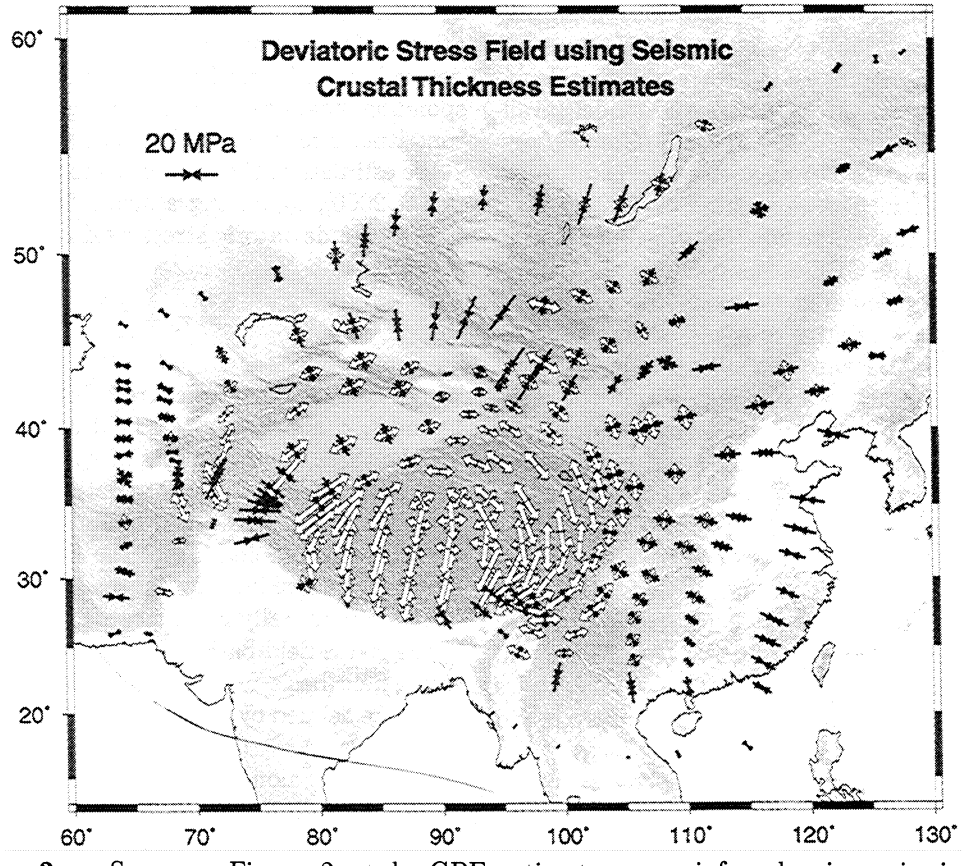

Figure 2c. Same as Figure 2a only GPE estimates were inferred using seismic crustal thickness estimates determined from surface wave data in Asia (G. Laske and G. Masters, http://mahi.ucsd.edu/Gabi/sediment.html, 2000).

formed on and close to the boundary of the grid to satisfy the requirement that $\Lambda = (\lambda_x, \lambda_y) = 0$ at all points on the boundary ∂S. Therefore we were careful to construct a grid such that boundaries followed regions of low GPE everywhere. The absolute magnitude of the deviatoric stress field is, however, influenced by the magnitude of the average crustal density, with higher average crustal densities yielding larger deviatoric stresses. For example, an increase in average crustal density for all crust of 100 kg/m^3 results in a 25% increase in deviatoric stress magnitudes but again does not affect the pattern of the deviatoric stress field, only the magnitude.

Upper mantle P_n velocities vary across Tibet by ~3% corresponding to a temperature variation of 240°C to 370°C [*McNamara et al.*, 1997]. Seismic evidence suggests that lithospheric thickness probably varies across Tibet and other parts of Asia [*Brandon and Romanowicz*, 1986; *McNamara et al.*, 1997; *Owens and Zandt*, 1997; *Rogers and Schwartz*, 1998; *Kosarev et al.*, 1999], indicating that our simplified model of uniform density mantle and perfect local Airy isostatic compensation may not apply everywhere. However, recent estimates of GPE variations in the western United States [*Jones et al.*, 1996] and Tibet [*England and Molnar*, 1997b] indicate that errors introduced by ignoring such variations in mantle density are relatively small in comparison with the total magnitude of the GPE signal obtained from the crustal contribution.

Since the estimation of GPE variations using the Airy isostasy assumption involves probable errors, we also calculate GPE estimates and corresponding deviatoric stress fields using the EGM96 geoid model (available from NIMA at http://164.214.2.59/GandG/wgs-84/egm96.html) (Figure 2b) and seismic crustal thickness estimates from surface wave data (G. Laske and G. Masters, http://mahi.ucsd.edu/Gabi/sediment.html, 2000) (Figure 2c). The GPE estimates using the EGM96 geoid model were calculated following the method of *Coblentz et al.* [1994] relative to a mid-ocean ridge column of lithosphere. Because of a signature in the geoid model from heterogeneities from deep within the mantle [*Hager et al.*, 1985], we removed terms below degree and order 7 with a cosine taper to degree and order 11 from the EGM96 geoid model [*Jones et al.*, 1996; *Sheehan and Soloman*, 1991]. GPE estimates from seismic crustal thickness estimates were calculated by again assuming a constant crustal and mantle density of 2828 and 3300 kg/m^3, respectively, and integrating density over each column of lithosphere using (3). These two methods of calculating GPE resulted in similar styles and magnitudes of deviatoric stresses (Figures 2b and 2c) to that obtained from the Airy isostatic case (Figure 2a), (i.e., compressional deviatoric stress normal to the Himalaya, fanning of compressional deviatoric stresses around the Tibetan Plateau, and N-S and E-W tensional deviatoric stresses within Tibet). However, second-order differences between the three solutions can be observed. Differences between the three deviatoric stress fields associated with the three GPE estimates (Figures 2a-2c) illustrate the inherent uncertainties in both magnitude and direction associated with the imprecise knowledge of the true distribution of GPE.

3. Stress Boundary Conditions and the Total Deviatoric Stress Field in Asia

We are working from the hypothesis that there are two major factors influencing the deformation field in Asia: (1) contributions to deviatoric stress from GPE differences within the lithosphere, which we have determined in section 2 and (2) deviatoric stress resulting from relative plate motion, which provides a stress field boundary condition. If this hypothesis is correct, then the stress field boundary condition, when added to the deviatoric stress field associated with GPE differences in the lithosphere, should provide a total deviatoric stress field that is compatible with the present-day deformation in Asia. Since the differential equations (2a) and (2b) are linear in stress, any number of solutions can be superimposed, regardless of rheology. Stresses resulting from individual tectonic sources and internal buoyancy effects (body forces) can be added linearly. What does not add linearly with nonlinear (a non-Newtonian) rheology is strain rate. Therefore it is legitimate to seek a second solution to the force balance equations corresponding to the stress boundary condition, which can be added to the contribution in stress from GPE variations. Only after the total deviatoric stress field is determined is it legitimate to address what the corresponding strain rates would be, given the appropriate constitutive relationship between stress and strain rate.

We estimate τ, the total deviatoric stress field [*Flesch et al.*, 2000], by adding a stress field boundary condition to the deviatoric stress field associated with GPE variations:

$$\tau = \tau_o + \sum_{i=1}^{3} a_i \tau_i, \tag{8}$$

where τ_o is the deviatoric stress field related to GPE differences, τ_i are three stress field basis functions, and a_i are the three scaling factors of τ_i. The deviatoric stress field associated with GPE variations (section 2) is used to calibrate the stress field boundary conditions, which are a linear combination of the three stress field basis functions determined by the scaling factors a_i. Therefore we are initially not concerned with the magnitudes of the stress field basis functions, only style. The three stress field basis functions that we have chosen to include are defined by assigning the values of the Lagrange multipliers, $\Lambda = (\lambda_x, \lambda_y)$, which have units of stress times length, along the boundaries of the Indian plate to be like velocity values in kinematic boundary conditions of rigid motion relative to Eurasia. The three sets of Lagrange multipliers defined along the Indian plate boundary, used to generate the three stress field

basis functions, are obtained using $\Lambda_i = \Omega_i \times \mathbf{r}$, where $\mathbf{r}$ marks the radial position along the Indian plate boundary and Ω_i are three orthogonal unit radial vectors, having units of stress, oriented at (0°N, 0°E), (0°N, 90°E), and (90°N, 0°E). We then minimize stress in (7) inside the region of interest with $\overline{\sigma}_{zz}$ set to zero. In determining the stress field basis functions we are only solving for a deviatoric stress field within the interior of our grid.

The three scaling factors a_i that define the linear combination of the three basis functions are determined in an iterative inversion such that the total deviatoric stress field τ matches as close as possible in style with the true stress tensor field. Since the true stress tensor field is not known, we infer an isotropic relationship between stress and strain rate in which case the stress tensor style is the same as the strain rate tensor style. We therefore use the style of the strain rate tensor obtained from Quaternary strain rates [*England and Molnar*, 1997a; *Holt et al.*, 2000a, 2000b] (open principal strain rate axes in Figure 1b) as our expected stress tensor style. The objective function that is minimized in our inversion for a stress field boundary condition is

$$\sum_{\text{areas}} \{ET - e\tau\}\,\Delta S, \tag{9}$$

where

$$E = \sqrt{\dot{\varepsilon}_{xx}^2 + \dot{\varepsilon}_{yy}^2 + \dot{\varepsilon}_{zz}^2 + \dot{\varepsilon}_{xy}^2 + \dot{\varepsilon}_{yx}^2}$$

$$= \sqrt{2\dot{\varepsilon}_{xx}^2 + 2\dot{\varepsilon}_{xx}\dot{\varepsilon}_{yy} + 2\dot{\varepsilon}_{yy}^2 + 2\dot{\varepsilon}_{xy}^2},$$

$$T = \sqrt{\tau_{xx}^2 + \tau_{yy}^2 + \tau_{zz}^2 + \tau_{xy}^2 + \tau_{yx}^2}$$

$$= \sqrt{2\tau_{xx}^2 + 2\tau_{xx}\tau_{yy} + 2\tau_{yy}^2 + 2\tau_{xy}^2},$$

$$e\tau = \tau_{xx}\dot{\varepsilon}_{xx} + \tau_{yy}\dot{\varepsilon}_{yy} + \tau_{zz}\dot{\varepsilon}_{zz} + \tau_{xy}\dot{\varepsilon}_{xy} + \tau_{yx}\dot{\varepsilon}_{yx}$$

$$= 2\tau_{xx}\dot{\varepsilon}_{xx} + \tau_{xx}\dot{\varepsilon}_{yy} + \tau_{yy}\dot{\varepsilon}_{xx} + 2\tau_{yy}\dot{\varepsilon}_{yy} + 2\tau_{xy}\dot{\varepsilon}_{xy},$$

where all stress tensor terms, τ, used above are from

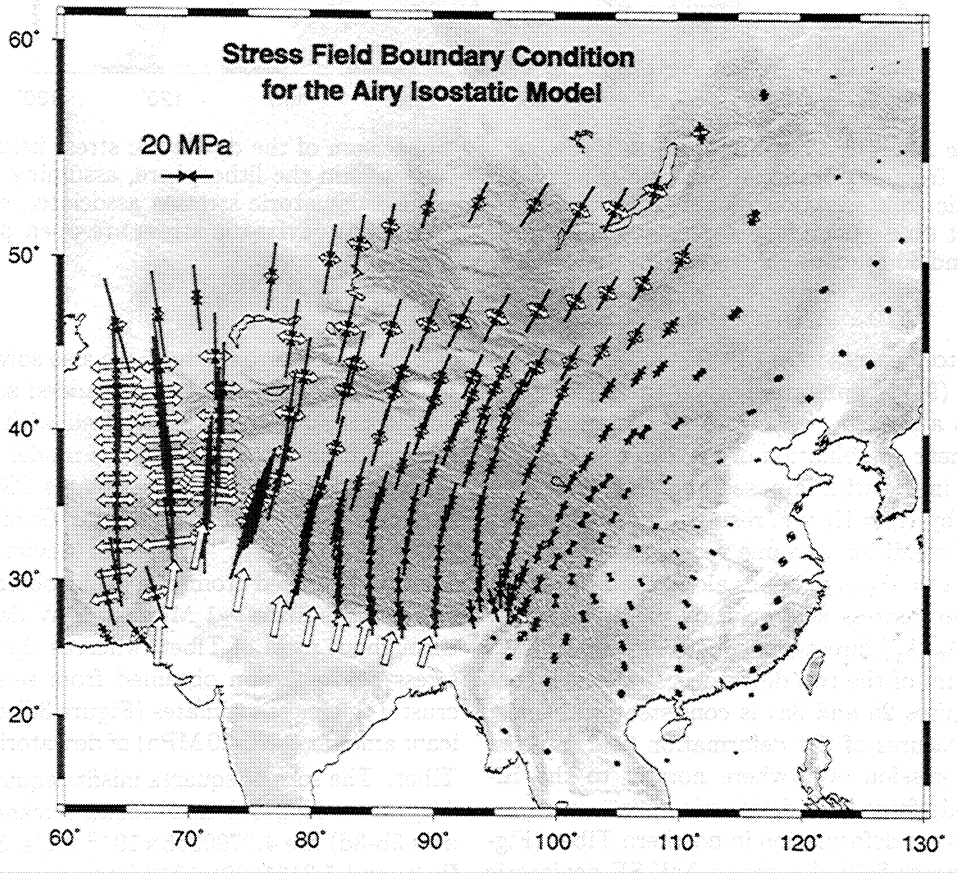

Figure 3a. The best fit far-field deviatoric stress contribution from a stress boundary condition defined by λ_α values, with units of stress times length, along the India boundary (shown as open vectors), with 3 degrees of freedom. The linear sum of this far-field deviatoric stress field and the one associated with gravitational potential energy differences (Figure 2a) provides the best fit to the style of present-day stress indicators (strain rate tensor field inferred from Quaternary fault slip rates, shown as open principal strain axes in Figure 1b) and is shown in Figure 3b. Tensional and compressional principal axes of deviatoric stress are represented by open and solid arrows, respectively.

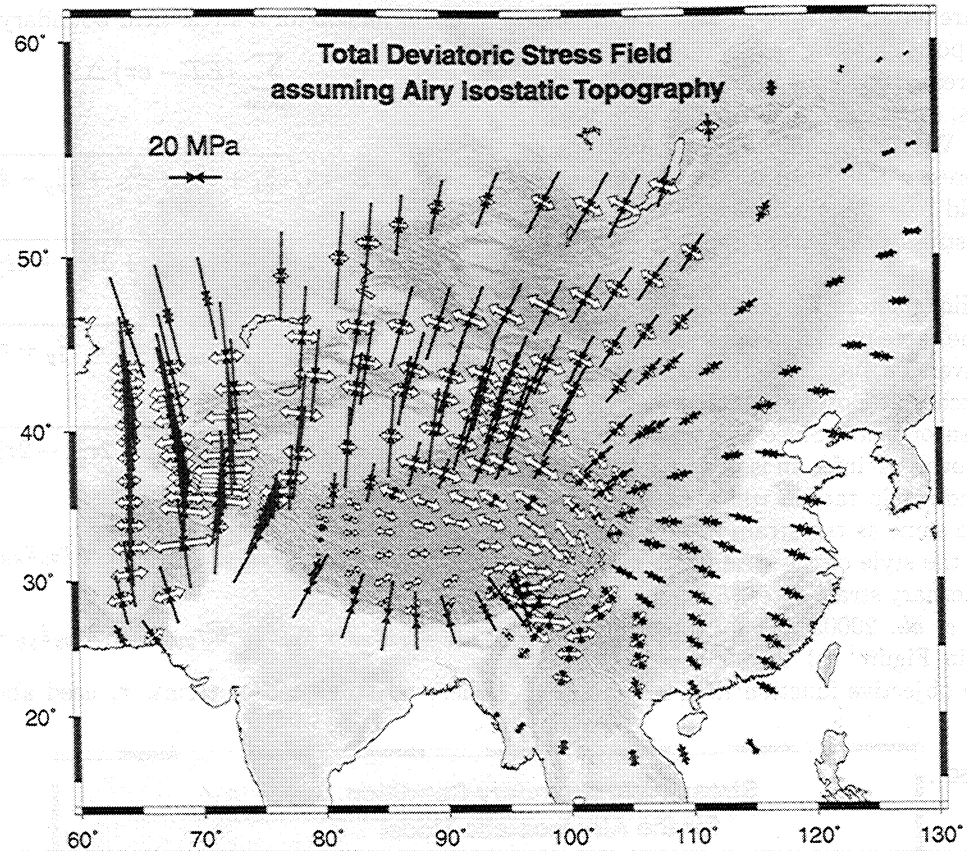

Figure 3b. Total deviatoric stress field that is a linear sum of the deviatoric stress field contribution from gravitational potential energy differences within the lithosphere, assuming an Airy isostatic compensation model (Figure 2a), and far-field deviatoric stresses associated with the best fit stress boundary conditions (Figure 3a). Tensional deviatoric stress are open principal axes and compressional deviatoric stresses are solid principal axes.

the total deviatoric stress from (8). The objective function (equation (9)) is minimized when the style of the stress tensor is a best fit to the style of the strain rate tensor. The linear combination of the three stress field basis functions in (8), with imposed Lagrange multiplier values defined by $\Lambda_i = \Omega_i \times \mathbf{r}$, results in a single stress field boundary condition and one vector Ω. The vector that gives the $\Lambda = (\lambda_x, \lambda_y)$ values along the boundaries for this deviatoric stress field solution yields relatively uniform $\Lambda = (\lambda_x, \lambda_y)$ directions (Figure 3a) of 20°-25°.

The linear sum of the two deviatoric stress field contributions (Figures 2a and 3a) is consistent with most of the major features of the deformation field in Asia, including compression everywhere normal to the Himalaya mountain front, and deviatoric stresses compatible with strike-slip deformation in northern Tibet (Figure 3b). The stress field also shows NW-SE deviatoric tension in east Tibet, approximately E-W deviatoric tension and N-S compression in southwestern China, and compression everywhere normal to the topographic front around the plateau of Tibet (Figure 3b). Vertically averaged values of absolute deviatoric stress magnitudes in the total solution are 5-40 MPa, with maximum deviatoric stress magnitudes in the Tarim Basin, southern Kazakh platform, and parts of Pakistan.

Using the above method, we also solve for stress field boundary conditions that are added separately to the deviatoric stress fields associated with GPE estimates inferred from the EGM96 geoid model (Figure 2b) and seismic crustal thickness estimates (G. Laske and G. Masters, http://mahi.ucsd.edu/Gabi/sediment.html, 2000) (Figure 2c). The total deviatoric stress field solution obtained from the geoid observations (Figure 3c) displays little, ~1 MPa, of E-W deviatoric tension throughout most of Tibet, whereas the total deviatoric stress field solution obtained from seismically defined crustal thickness estimates (Figure 3d) displays a significant amount (~10-20 MPa) of deviatoric tension within Tibet. The sum of squares misfit (equation (9)) for the Airy isostatic, geoid, and crustal thickness models (Figures 3b-3d) are 4.0700356×10^{-2} Pa/s, 3.1109144×10^{-2} Pa/s, and 5.3131020×10^{-2} Pa/s, respectively.

Although the three total deviatoric stress fields (Figures 3b-3d) show comparable deviatoric stress magnitudes, local differences in style and magnitude of deviatoric stress between the three solutions illustrate the level of uncertainty in our initial estimate of the total deviatoric stress field. The two primary sources of uncertainty are embedded in the inexact knowledge of the GPE distribution and the simple stress boundary treat-

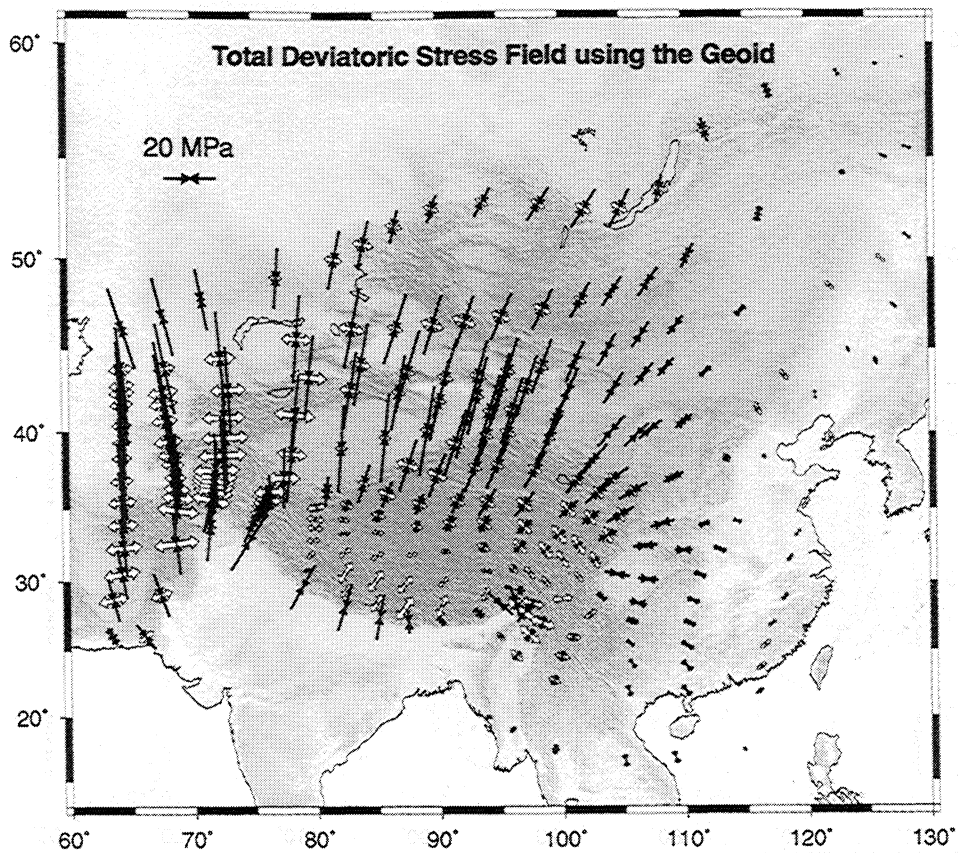

Figure 3c. The total deviatoric stress field as described in Figure 3b, only deviatoric stresses associated from GPE variations were determined using the EGM96 geoid model (Figure 2b) to solve for the deviatoric stress field boundary conditions.

ment we use (with only 3 degrees of freedom, a_i). Our stress boundary treatment accounts on a broad scale for deviatoric stresses associated with the relative convergence of India and Eurasia but, for instance, makes no explicit allowance for interaction of eastern Asia with the Pacific and Phillipine Sea plates. An area where the relative magnitudes and directions of deviatoric stresses do not fit the observables well is in Baikal and neighboring parts of Mongolia. Figure 3b shows very little if any deviatoric tension in Baikal, while it is clear from Figure 1a that extension is occurring there, though at slow rates (Figure 1b) [*England and Molnar*, 1997a; *Calais et al.*, 1998].

4. Vertically Averaged Effective Viscosity in Asia

Since we have been able to determine vertically averaged deviatoric stresses of a minimum absolute magnitude that solve equations (2a) and (2b), it is now possible to obtain a corresponding minimum vertically averaged effective viscosity $\overline{\eta}$ of the lithosphere in Asia for the case of a simple isotropic relationship between stress and strain rate:

$$\overline{\tau}_{\alpha\beta} = \overline{\eta}\dot{\varepsilon}_{\alpha\beta}. \tag{10}$$

We estimate $\overline{\eta}$ by dividing the magnitude $T = \sqrt{\tau_{\alpha\beta}\tau_{\alpha\beta} + \tau_{\gamma\gamma}^2}$ (in equation (9)) of the deviatoric stress field in Figure 3b by the equivalent invariant $E = \sqrt{\dot{\bar{\varepsilon}}_{\alpha\beta}\dot{\bar{\varepsilon}}_{\alpha\beta} + \dot{\varepsilon}_{\gamma\gamma}^2}$ of the strain rate. For generally nonlinear viscous behavior,

$$\overline{\eta} = BE^{1/n-1}, \tag{11}$$

where n is the power law exponent and B is a constant sensitive to temperature [*England and McKenzie*, 1982; *Sonder and England*, 1986]. Regional strain rates obtained from the joint fitting of Quaternary fault slip rates and GPS data (solid vectors in Figure 1b) [*England and Molnar*, 1997a; *Holt et al.*, 2000a, 2000b] are used to determine the values of effective viscosity $\overline{\eta}$ for the Newtonian case (n=1, $\overline{\eta} = B$) (Plate 1a), and the B values for the power law rheology n=3 and n=5 cases (Plates 1b and 1c). The vertically averaged effective viscosity for Tibet is relatively uniform at 0.5-5 $\times 10^{22}$ Pa s (Plate 1a). Values of vertically averaged effective viscosity are larger within block-like regions outside of Tibet, such as southern China and Tarim Basin with values about 1-2$\times 10^{23}$ Pa s. North of the deformation in Tien Shan, in the Kazakh platform, and within the Amurian block, vertical averages of effective viscosity

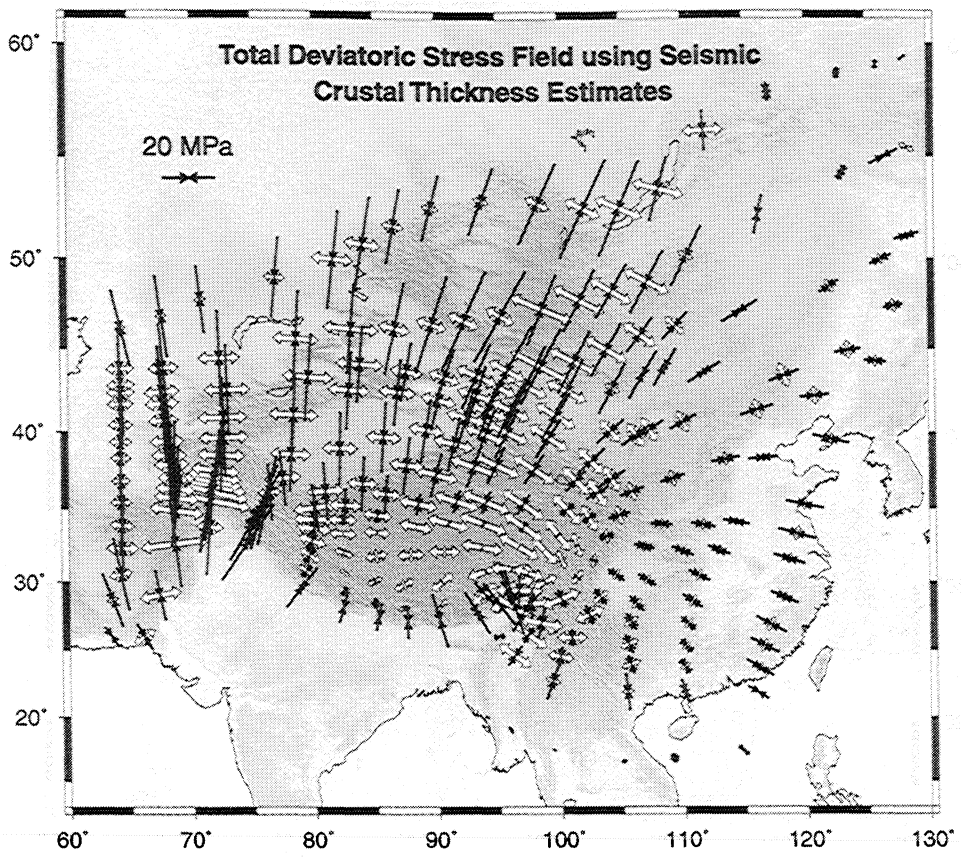

Figure 3d. The total deviatoric stress field as described in Figure 3b, only deviatoric stresses associated from GPE variations were determined using the seismic crustal thickness data (G. Laske and G. Masters, http://mahi.ucsd.edu/Gabi/sediment.html, 2000) (Figure 2c) to solve for the stress field boundary conditions.

are around 1-2.5×10^{23} Pa s. Our values of vertically averaged effective viscosity for Tibet are consistent with the single average of 1-2×10^{22} Pa s obtained by *England and Molnar* [1997b]. As the value of n increases, the variation in the B value throughout the region decreases (Plates 1b and 1c). Low strain rates in south China and eastern Indo-China, even though B values are relatively low there, are explained by the small deviatoric stress magnitude there. For both cases of n=3 and n=5, Tibet and South China, as well as the region around Lake Baikal, are relatively uniform with low B values. As in the Newtonian case, B values increase moving away from Tibet with the highest B values found in the Tarim Basin and the shield region farther north (Plates 1b and 1c).

Using a Monte Carlo type approach, we estimated the uncertainties in the vertically averaged viscosity. We first assumed a 1σ value of $\overline{\sigma}_{zz}$ for any given area to be equal to ±10% of the GPE differences between Tibet and south China ($\pm 7.3 \times 10^6$ N/m^2 or $\pm 7.3 \times 10^{11}$ N/m). We then performed a realization of new GPE estimates for the 250 areas followed by a calculation of a new deviatoric stress field estimate. A total of 300 such deviatoric stress fields were determined (associated with the 300 different realizations of GPE distributions), and the standard deviation in deviatoric stress for each area was calculated. The average standard deviation in the total deviatoric stress field was ~±20%. Using these values for standard error in total deviatoric stress and using the formal variances in strain rates obtained in the kinematic solution [*Holt et al.*, 2000b], the average standard error in viscosity is ~±40%.

We can investigate the implications that our vertical averages of viscosity have for the strength of the lithosphere at various depths. This is a nonunique problem, and therefore we consider three possible cases from published strength profiles [e.g., *Molnar*, 1992; *Kohlstedt et al.*, 1995]. From a strength profile we construct a dimensionless viscosity:

$$\widetilde{\eta}(z) = \frac{\eta(z)}{\frac{1}{h}\int_0^h \eta(z)dz}, \tag{12}$$

where $\eta(z)$ is the relative viscosity distribution with depth, inferred from the strength profile, h=100 km, and $\int_0^h \widetilde{\eta}(z)dz = h$. Because $\widetilde{\eta}(z)$ is a normalized viscosity, the absolute magnitudes of the strength profile do not matter; what is important is the shape of the proflie (i.e., the integral of the area under the strength curve). Using the dimensionless viscosity $\widetilde{\eta}(z)$, it is pos-

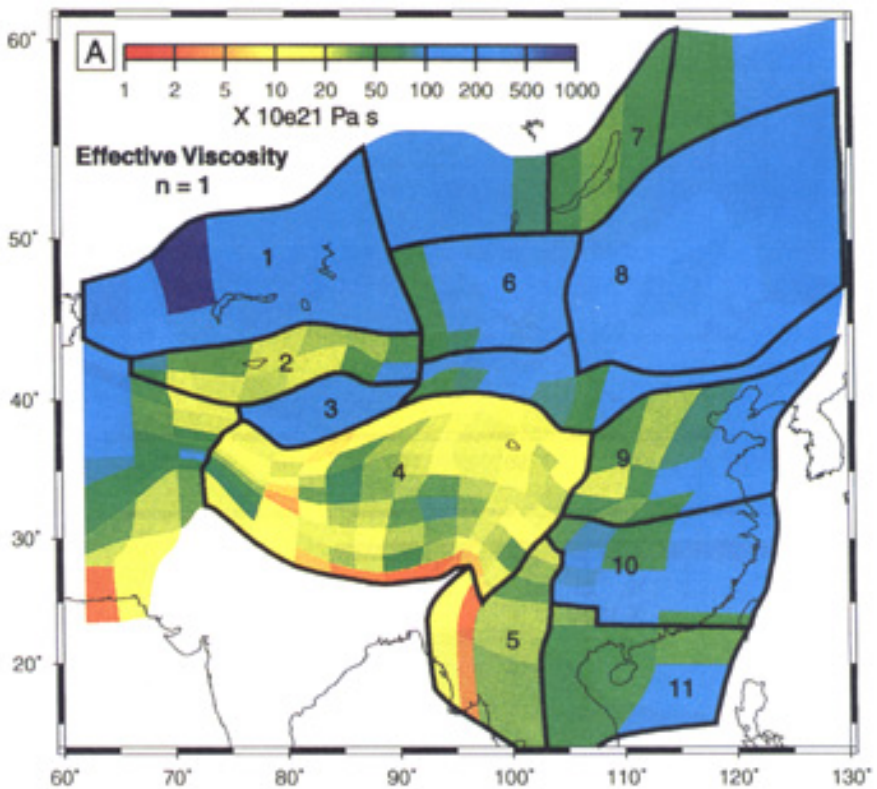

Plate 1. (a) Vertically averaged effective viscosity for Asia obtained by taking the magnitude of vertically averaged deviatoric stresses in areas in Figure 3b and dividing by the magnitude of average strain rates in same areas. The magnitude of strain rates were those inferred from the matching of Quaternary fault slip rates and GPS velocities (solid arrows, Figure 1b). Numbered areas refer to Table 1. (b) Vertically averaged B values for Asia obtained by taking the vertically averaged viscosities in areas in Plate 1a, the magnitude of the model average strain rates E in same areas in Figure 1b (solid arrows), and using equation (11), assuming n=3. (c) Vertically averaged B values for Asia, as described in Plate 1b, except for the case where n=5.

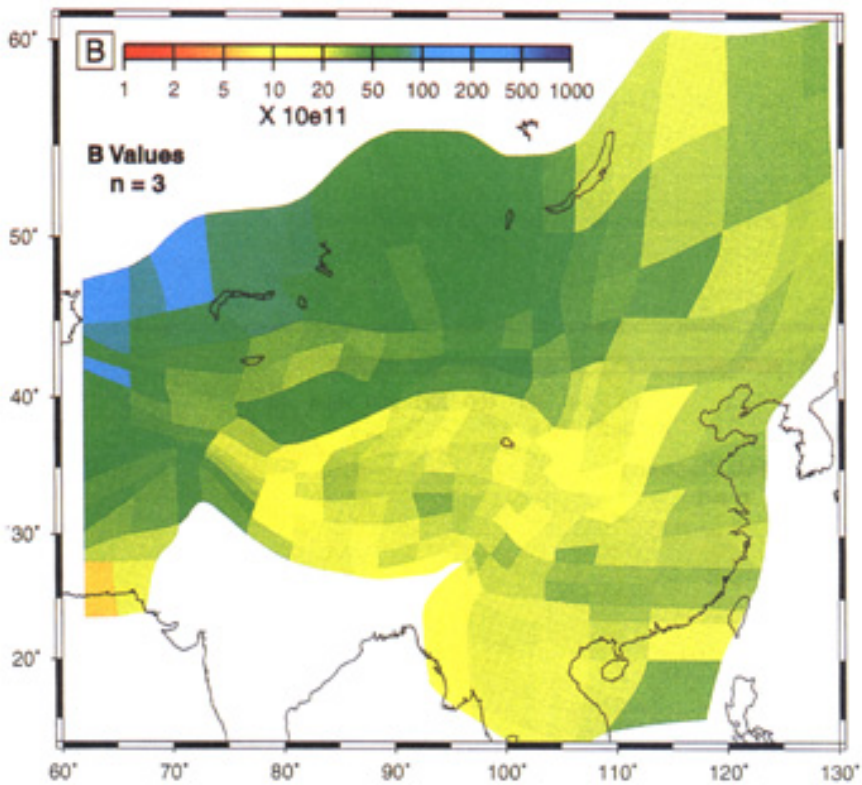

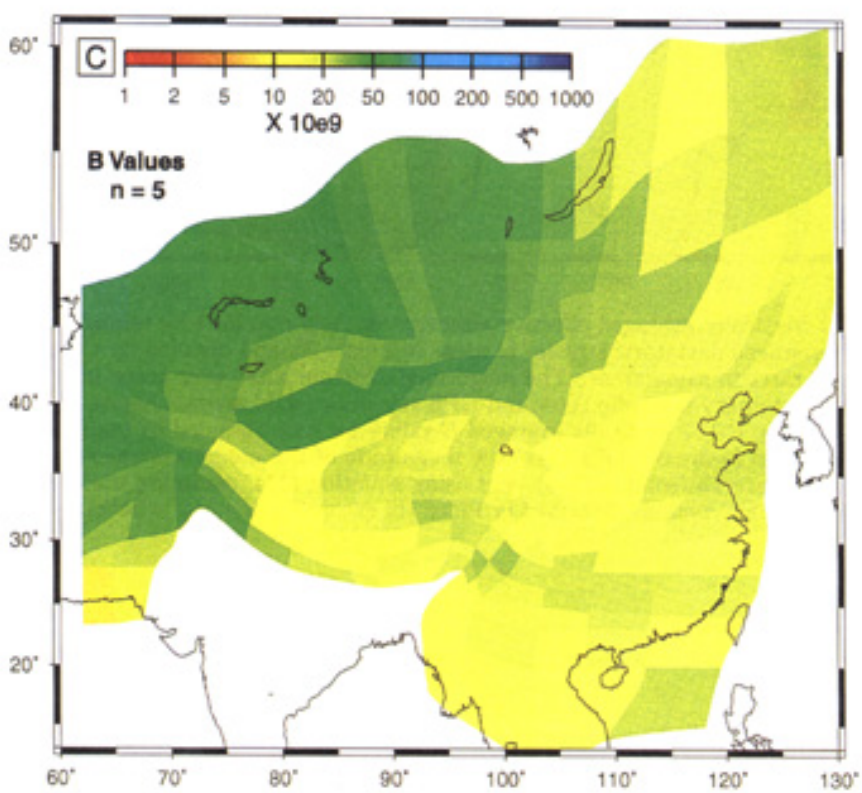

Plate 1. (continued)

Table 1. Average for Effective Viscosity (n=1) and B values for the Different Regions Shown in Plate 1a[a]

	Area	n=1; it=1, 10^{21} Pa s	n=3; it=1, 10^{11} Pa $s^{\frac{1}{3}}$	n=5; it=1, 10^{9} Pa $s^{\frac{1}{5}}$	n=3; it=2, 10^{11} Pa $s^{\frac{1}{3}}$	n=5; it=2, 10^{9} Pa $s^{\frac{1}{5}}$
Kazakh Platform	1	242	78	63	66	54
Tien Shan	2	50	42	42	34	35
Tarim Basin	3	124	59	51	58	50
Tibet	4	23	20	20	20	20
SW China	5	23	17	16	17	16
West Mongolia	6	120	45	38	44	37
Lake Baikal	7	51	30	27	24	24
Amurian Block	8	150	32	23	37	25
NE China	9	75	23	18	29	21
South China	10	110	26	20	31	20
South China Sea	11	75	22	17	21	17

[a]Here n is the assumed power law exponent, it=1 represents the initial minimum estimate of B value from Plates 1b and 1c, and it=2 represents the updated B value after the first iteration of forward modeling from Plates 2a and 2b.

sible to infer the magnitude of the deviatoric stress value at a given depth, $\tau(z) = \widetilde{\eta}(z)\overline{\tau}$, where $\overline{\tau}$ is the vertically averaged deviatoric stress magnitude from our solution. The first profile, of the three strength profiles we have considered, ignores any contribution from the mantle, and the distribution of deviatoric stress in the crust is given by the strength profile constructed by *Kohlstedt et al.* [1995] using the activation energy reported by *Kronenberg and Tullis* [1984] and *Luan and Paterson* [1992]. The second profile (wet rheology) has roughly equal contributions in integrated strength from both crust and mantle and is obtained from the above crustal strength profile plus the mantle profile reported by *Kohlstedt et al.* [1995]. Finally, the third profile (dry rheology taken from *Molnar* [1992]) has the dominant contribution to the integral of strength from the mantle. At depths of 5-10 km in Tibet, profiles 1 and 2 predict deviatoric stress magnitudes T of 100-160 MPa and 70-120 MPa, respectively. Profile 3, where the majority of integrated strength comes from the mantle, predicts deviatoric stresses at depths of 5-10 km of 12-26 MPa within Tibet. Within the Tien Shan, profiles 1 and 2 predict deviatoric stress magnitudes of 200-370 MPa at depths of 5-10 km, whereas profile 3 predicts 34-73 MPa of total deviatoric stress magnitude at these same depths. The higher deviatoric stress values obtained from profiles 1 and 2 for the seismogenic portion of the crust are in agreement with stress magnitudes predicted by laboratory and theoretical friction experiments [e.g., *Sibson*, 1982; *Kohlstedt et al.*, 1995]. On the other hand, if most of the strength lies within the mantle portion of the lithosphere [*Molnar*, 1992], then our vertical averages imply that deviatoric stress values within the seismogenic portion of the crust are expected to be of the same order of magnitude as the stress drops of intraplate earthquakes [*Kanamori and Anderson*, 1975]. In order for our vertical averages of deviatoric stress to be consistent with observed data and experimental results [*Sibson*, 1982; *Kohlstedt et al.*, 1995; *Brudy et al.*, 1997], a significant portion of the strength of the lithosphere is implied to reside within the seismogenic portion of the crust [e.g., see *Maggi et al.*, 2000], with peak values of deviatoric stress of 100-300 MPa within this zone.

5. Forward Modeling

We perform standard forward modeling to refine the dynamic calculations, using velocity boundary conditions as opposed to the approximation of the stress boundary conditions, with a specified distribution of body forces (GPE variations), and a defined distribution of vertically averaged effective viscosities. Forward modeling requires one to assume or "guess" the viscosity or B value distribution, which is a function of strain rate. However, our initial estimates of deviatoric stress in Figure 3b, and the associated vertically averaged effective viscosity estimates in Plate 1, now provide important initial constraints for forward modeling.

In Appendix C we demonstrate the standard result that with a defined distribution of viscosity, body forces, and velocity boundary conditions the minimization of

$$\Theta = \int\int_s [D - \nu_\alpha f_\alpha]\, dxdy \qquad (13)$$

with respect to the velocity fields and associated strain rates provides associated deviatoric stresses that solve the force balance equations [*Hildebrand*, 1952; *Bird*, 1960], where f_α is the body force term associated with the gradients of gravitational potential, ν_α is the velocity, and D is the dissipation potential. The dissipation potential is a function of the B value, the strain rates, and the power law exponent n,

$$D = \frac{n}{n+1} B \left(\dot{\varepsilon}_{\alpha\beta}\dot{\varepsilon}_{\alpha\beta} + \dot{\varepsilon}_{\gamma\gamma}\dot{\varepsilon}_{\gamma\gamma}\right)^{\frac{n+1}{2n}}, \qquad (14)$$

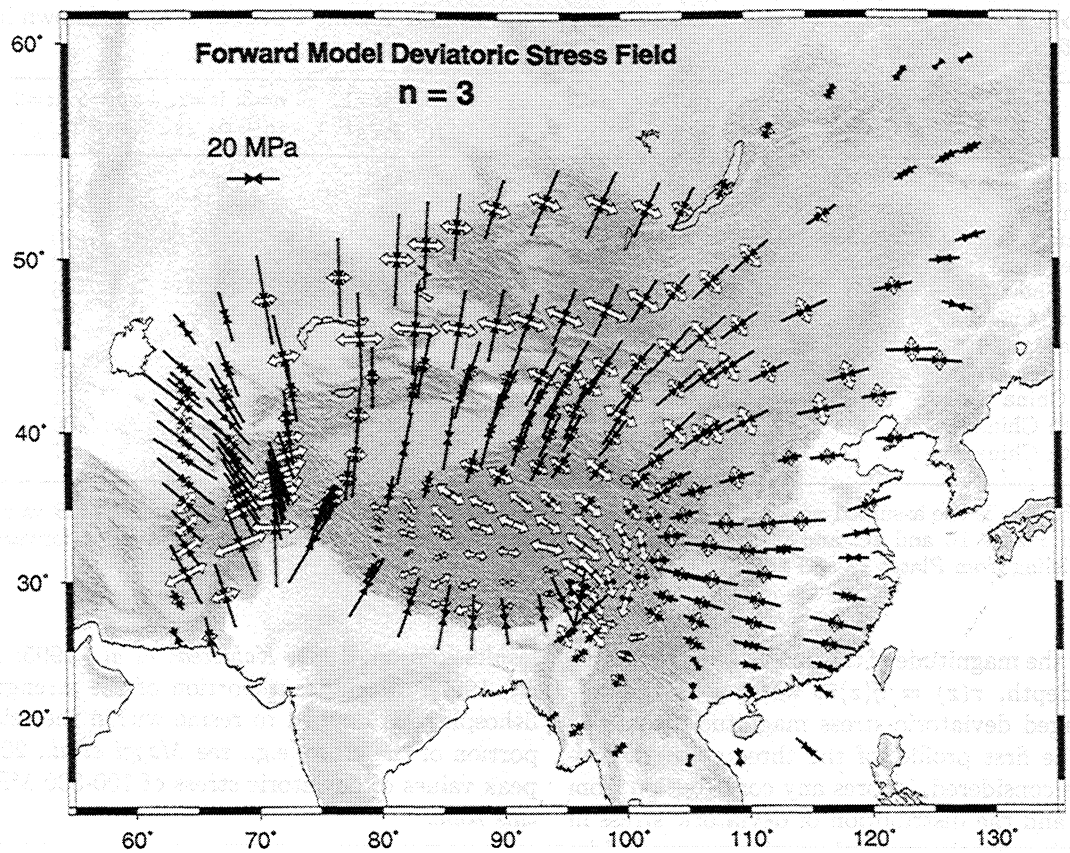

Figure 4a. Forward modeled total deviatoric stress field assuming a power law rheology where n=3 determined by minimizing equation (13) subject to the velocity boundary condition [*Holt et al.*, 2000b]. The distribution of $\overline{\sigma}_{zz}$ values is the same as that used to infer deviatoric stresses in Figure 2a, and the distribution of viscosity values is the same as that in Plate 2a. Format for compressional and tensional deviatoric stresses is the same as that used in Figures 2a-2c.

where $\dot{\varepsilon}_{\gamma\gamma} = (\dot{\varepsilon}_{xx} + \dot{\varepsilon}_{yy}) = -\dot{\varepsilon}_{zz}$. Using $f_\alpha = \partial\overline{\sigma}_{zz}/\partial x_\alpha$, making use of the product rule, and then applying the divergence theorem, (13) becomes

$$\Theta = \int\int_S [D + \dot{\varepsilon}_{\gamma\gamma}\overline{\sigma}_{zz}]\, dxdy - \int_{\partial S} \nu_\alpha \overline{\sigma}_{zz} n_\alpha d\ell. \quad (15)$$

The second term in (15) involves a velocity boundary condition ν_α around the boundary of ∂S ($dxdy$) and the GPE, $\overline{\sigma}_{zz}$. In the minimization of Θ the velocity boundary conditions are held fixed along $d\ell$, and the GPE and the B value distribution also remain fixed within the interior of the grid to obtain the velocity, strain rate, and deviatoric stress fields inside of S. We initially use the B value distribution that we obtained in section 4 (values plotted in Plates 1b and 1c), in the forward modeling in (15), as well as the assumed distribution of GPE, $\overline{\sigma}_{zz}$, used in section 2 to infer the deviatoric stress field solution in Figure 2a. We apply the velocity boundary conditions, ν_α, relative to Siberia (which are shown in Figure 1c), obtained from the inversion of Quaternary strain rates and GPS velocities [*Holt et al.*, 2000b], to the Indian plate and the western and eastern boundaries in our forward modeled grid. Along the northern boundary of the grid in Siberia points are stationary.

Using the distribution of B, and $\overline{\sigma}_{zz}$, we expand (15) about $\dot{\varepsilon}_{\alpha\beta}$ using a Taylor series polynomial (see Appendix D for details), and iteratively minimize $\dot{\varepsilon}_{\alpha\beta}$ in the expanded function under the imposed velocity boundary conditions holding the B values, $\overline{\sigma}_{zz}$, and ν_α constant until $\dot{\varepsilon}_{\alpha\beta}$ converged. This was done for n values of 3 and 5, using a finite element approach to solve for a forward modeled deviatoric stress, strain rate, and velocity field. To refine our estimates of deviatoric stress and effective viscosity, we divide the magnitude of our new forward modeled deviatoric stress field by the magnitude of the strain rates obtained from the joint fitting of Quaternary fault slip rates and GPS data (solid vectors in Figure 1b) [*England and Molnar*, 1997a; *Holt et al.*, 2000a, 2000b] to obtain a revised estimate of the B value distribution for a given value of n (see equations (10) and (11)). Using the updated B value distribution, $\overline{\sigma}_{zz}$ values from section 2, and velocity boundary conditions from the kinematic study, we again minimize $\dot{\varepsilon}_{\alpha\beta}$ in (15) to obtain a revised estimate of the deviatoric stress field. In both cases convergence occurred after the B values were updated for the first time. Regional averages of the B value distribution before and after the B values were updated are shown in

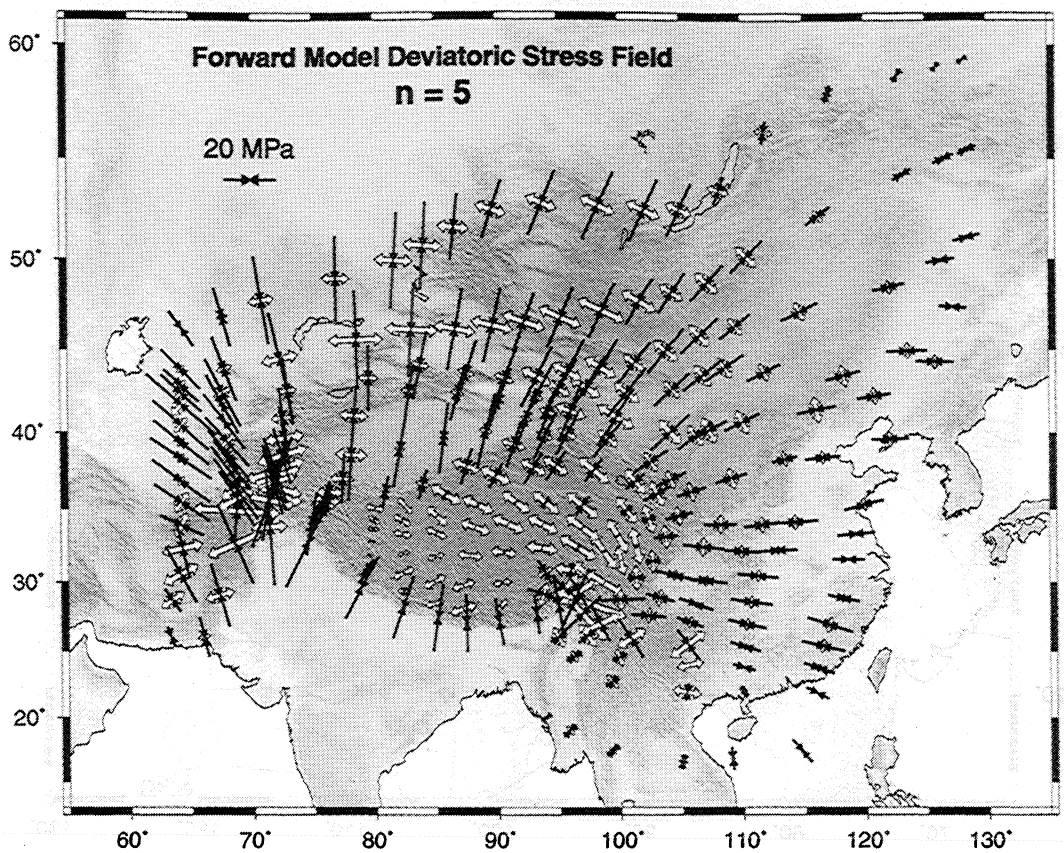

Figure 4b. Forward modeled total deviatoric stress field as described in Figure 4a except for a power law rheology where n=5, and B values from Plate 2b. Format for compressional and tensional deviatoric stresses is the same as that used in Figures 2a-2c. The similarity in deviatoric stress directions and deviatoric stress magnitudes in Figures 4a and 4b with those in Figure 3b indicate that our estimates of minimum absolute magnitudes of deviatoric stress in Figure 3b are not sensitive to the actual variations in effective viscosity in Asia, which are a few orders of magnitude. Furthermore, the forward modeled deviatoric stress is not sensitive to power law exponent (n=3 versus n=5).

Table 1, and the final B values for n=3 and n=5 are shown in Plates 2a and 2b.

Any differences between the deviatoric stress field solutions in Figures 4a and 4b are a result of errors in the assumed lateral viscosity distribution. If the exact distribution of apparent viscosity were known, then the deviatoric stress solutions would be independent of n. However, the fact that the forward modeled deviatoric stress fields yield similar patterns for $n = 3$ and $n = 5$ indicates that the initial assumed viscosity distribution (Plate 1 and Table 1) is a valid approximation, and the refined B values (Plate 2 and Table 1) are a reasonable representation of the actual viscosity distribution. Furthermore, for most regions the magnitudes of the forward modeled deviatoric stresses are within about a factor of 2 of the minimum deviatoric stress field magnitudes in Figure 3b. The similarity of deviatoric stress magnitudes for the case in which the minimum deviatoric stress is solved for directly versus the case in which the deviatoric stress field is solved for using the viscosity distribution in Plate 1 illustrates the insensitivity of deviatoric stress magnitudes to lateral variations in apparent viscosity or B value. Most of the differences in the total minimum deviatoric stress field estimate (Figure 3b) and the two forward modeled deviatoric stress fields (Figures 4a and 4b) arise from the inadequacy of the estimate of the stress field boundary condition (Figure 3a).

Note that the forward modeled deviatoric stress fields (Figures 4a and 4b) in Lake Baikal and neighboring regions now produce ~5-20 MPa of NW-SE deviatoric tension, a feature missing from the minimum deviatoric stress field calculation in Figure 3b. Recall that in solving for the stress boundary conditions we use only a first approximation involving specified values of the Lagrange multipliers applied only along the boundaries with the Indian and Eurasian plates. However, the velocity boundary conditions from the kinematic solution used in the forward modeling are a complete boundary condition in that they describe the accommodation of India-Eurasia relative plate motion, as well as motions along the eastern boundary that give rise to a more

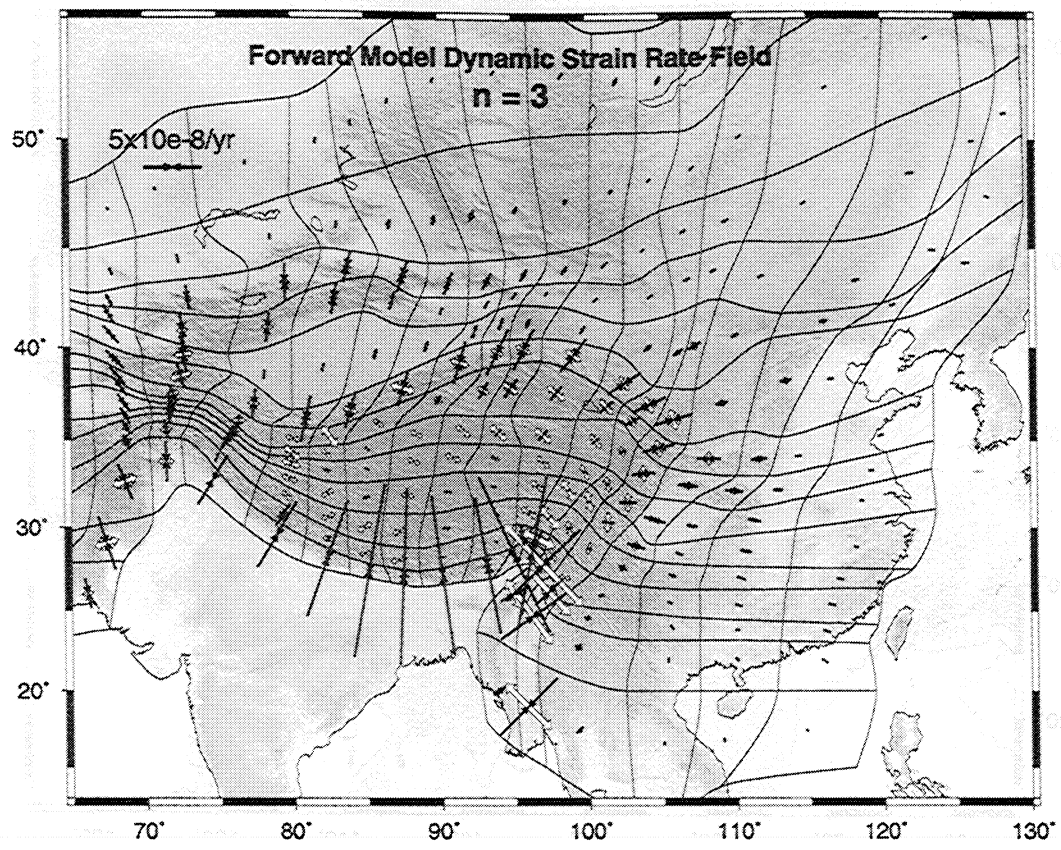

Figure 5a. Forward modeled strain rates associated with deviatoric stress field in Figure 4a (n= 3).

substantial component of NW-SE deviatoric tension in Mongolia, Baikal, and Amurian Block regions.

Strain rates determined in the forward modeling (Figure 5a) are similar to the strain rates inferred from the kinematic solution (Figure 1b), obtained from GPS and Quaternary fault slip rate data (see Table 2). Since strain rates are strongly dependent on the distribution of B value (whereas we have shown that deviatoric stress is not), the similarity of Figure 5a with Figure 1b (see Table 2) again indicates (assuming n=3) that our B value estimates (Plate 2a) are a reasonable representation of the actual distribution. In addition, this similarity indicates that the assumption of an isotropic relationship between stress and strain rate for the lithosphere is a reasonable approximation for most areas within Asia. Likewise, the velocity field from the dynamic model (Figure 5b) is similar (see Table 3) inside the region of interest to the kinematic velocity field and GPS measurements (Figure 1c). However, the dynamic velocity field does not produce the NNW motion of the Tarim Basin with respect to Eurasia that has been inferred from GPS data (Figure 1c). This NE motion of the Tarim Basin relative to Eurasia in Figure 5b is related to the minimal strike-slip motion produced by the dynamic deviatoric stress field along the Altyn Tagh fault. If the relationship between stress and strain rate along the Altyn Tagh fault zone were anisotropic, as opposed to isotropic, such a deviatoric stress field could produce left-lateral strike-slip motion, consistant with ~10 mm/yr of left-lateral slip on the Altyn Tagh fault [e.g., *Bendick et al.*, 2000]. A pure left-lateral strike-slip motion of ~10 mm/yr along the Altyn Tagh fault zone in the dynamic velocity field solution in Figure 5b would allow the Tarim Basin to move N-NW with respect to Eurasia.

We have also performed the forward modeling using the $\overline{\sigma}_{zz}$ values calculated using the EGM96 geoid model and seismic crustal thickness estimates (G. Laske and G. Masters, http://mahi.ucsd.edu/Gabi/sediment.html, 2000). Again both dynamic calculations (n=3 and n=5) produced similar fits to the strain rate tensor field (Table 2) and GPS data in a Eurasian framework (Table 3).

6. Discussion and Conclusions

We have inferred an initial estimate of the vertically averaged deviatoric stress field associated with GPE variations as well as deviatoric stresses associated with first-order stress boundary conditions. Constraints on the rates of strain that come from Quaternary fault slip rates are then taken together with estimates of the minimum absolute magnitude of deviatoric stress to infer distributions of vertically averaged effective viscosity

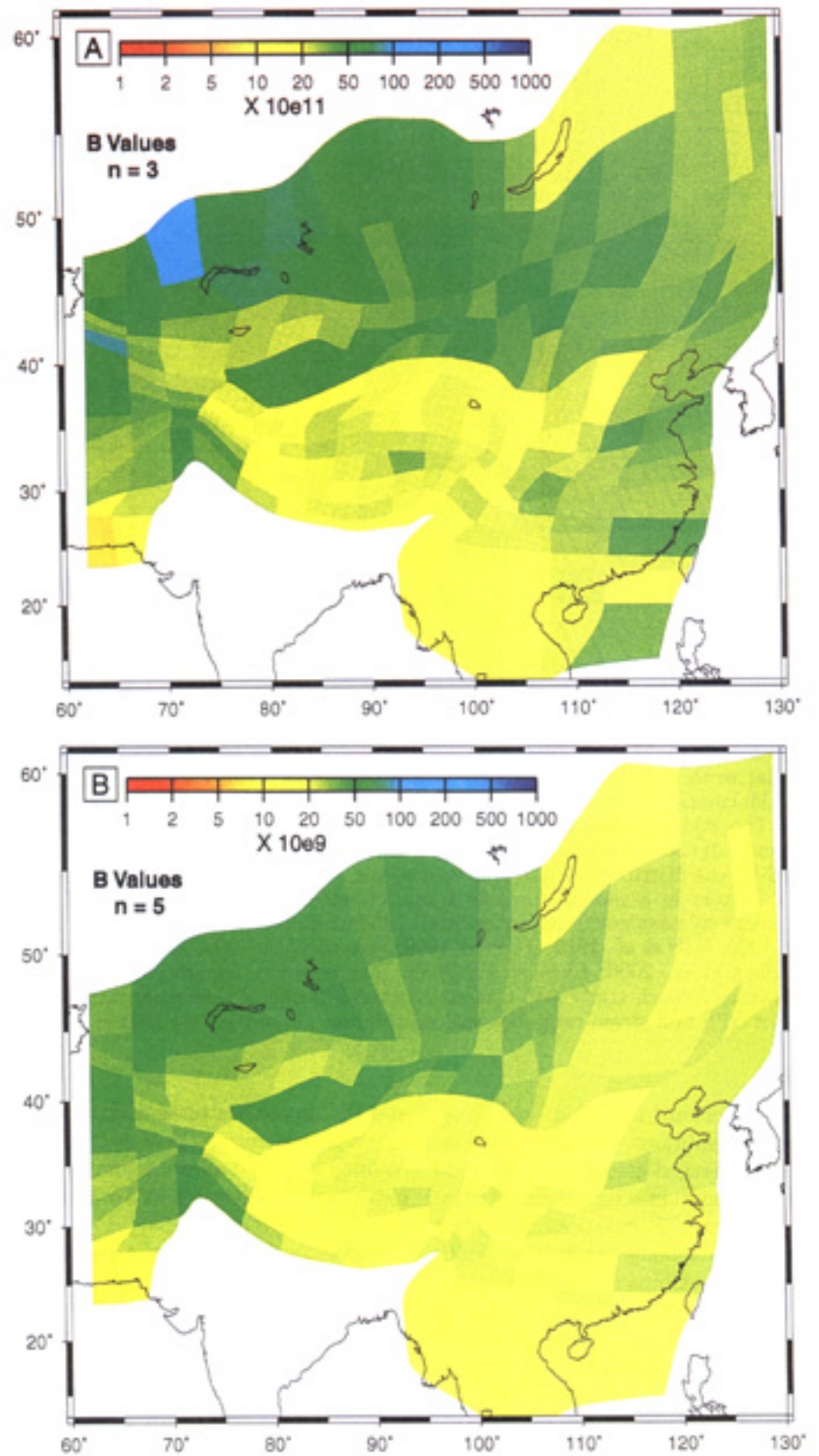

Plate 2. (opposite) (a) Refined vertically averaged B values for Asia, assuming n=3, obtained by taking the magnitude of the vertically averaged deviatoric forward modeled stress in areas and dividing by the magnitude of averaged strain rates in the same areas. The magnitude of strain rates were those inferred from the matching of Quaternary fault slip rates and GPS velocities (solid arrows, Figure 1b). (b) Same as Plate 2a, only assuming n=5.

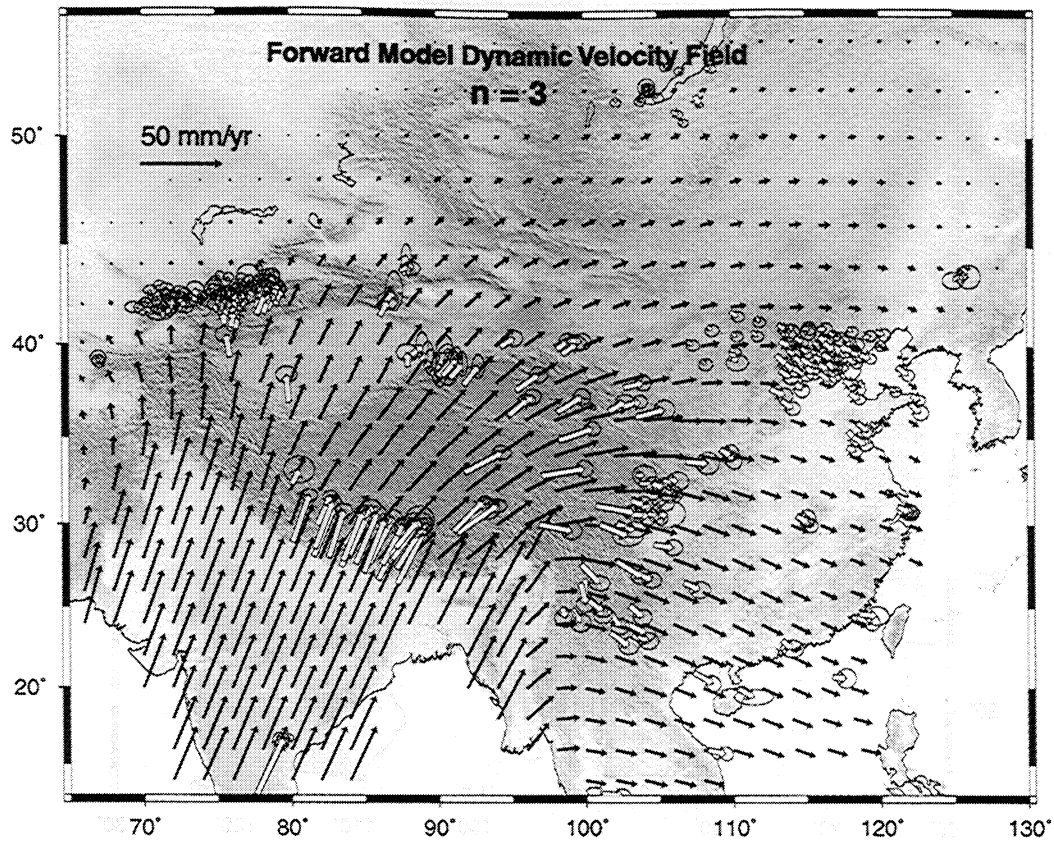

Figure 5b. Self-consistent velocity field associated with dynamic solution in Figures 4a and 5a, plotted relative to Eurasia. The velocity field within the interior regions (inside ∂S) closely resembles the kinematic solution inferred from both GPS observations and Quaternary slip rates (Figure 1c). The style of deformation indicators are not used to define the deviatoric stress tensor (and hence deviatoric strain rate tensor) in the dynamic solution. This dynamic solution is only defined by the distribution of $\overline{\sigma}_{zz}$, B values, and velocity boundary conditions. Observed GPS velocity vectors in a model Eurasian frame of reference are also shown (IGS available at http://sideshow.jpl.nasa.gov/mbh/series.html) [*Abdrakmatov et al.*, 1996; *Calais et al.*, 1998; *Larson et al.*, 1999; *Heki et al.*, 1999; *Yu et al.*,1999; *Simons et al.*, 1999; *Zhu et al.*, 2000; *Bendick et al.*, 2000; *Shen et al.*, 2000; *Chen et al.*, 2000]. The reference frames (rotation vectors that rotate observations in each study into a model Eurasian frame of reference) were solved for in the inversion of GPS and strain rate observations (Figures 1b and 1c [see *Holt et al.*, 2000b]).

and B values. Dynamic forward modeling, with kinematic velocity boundary conditions, yields a refined estimate of the vertically averaged deviatoric stress field and effective viscosity distribution. Our treatment of internal body forces related to GPE variations along with the inclusion of velocity boundary conditions, which contain E-SE motion of south China relative to Eurasia, yields ~E-W stretching throughout much of central and southern Tibet as well as NNW-SSE stretching east of the Eastern Syntaxis of the Himalaya (Figures 4 and 5). Our dynamic deviatoric stress field solution is consistent with the inference that the strains around the collision zone can be understood as the natural response of an effectively viscous material that is being influenced by India-Eurasia motion and that contains GPE differences associated with the compensation of present-day topography in Asia [*England and Housman*, 1986]. However, boundary conditions in the east, along the Pacific plate and Philippine Sea plate margins, also play an important role, influencing the style of deformation east of the collision zone and allowing south China and SE Asia to move eastward relative to Eurasia [*Burchfiel and Royden*, 1991; *Holt et al.*, 1995].

Our dynamic calculations enable us to quantify, over length scales that are several times the lithospheric thickness, the relative influence of deviatoric stresses needed to balance lateral density variations and deviatoric stresses imposed on the boundary of the thin sheet (lithosphere). However, our viscous approach does not exclude the possibility of block-like behavior for any portion of the lithosphere. Indeed, the dynamic solutions do identify zones of relatively high viscosity (Plate 1a and Table 1), which would behave like rigid blocks in regions such as Tarim Basin, Amurian Block, and most of south China. Our choice of grid size, along with the limited density of GPS observations, does not en-

Table 2. Goodness of Fit of Dynamic Strain Rate Solutions for Different Power Law Rheologies and Gravitational Potential Energy Estimate Models to Kinematic Strain Rate Solutions[a]

n	Model	Total SSM	DoF	RMS Misfit
3	Airy isostatic	1298.1	750	1.316
5	Airy isostatic	2922.2	750	1.974
3	geoid	916.0	750	1.105
5	geoid	1383.2	750	1.358
3	seismic	1427.6	750	1.380
5	seismic	3380.3	750	2.123

[a]SSM is the sum of squared misfit between the model and observed strain rate components. Each squared misfit in the summation is weighted by the variance in observed strain rate component. DoF is the number of degrees of freedom, which is equal to 3 times the number of grid areas. RMS misfit is the square root of the quantity of total SSM divided by the number of degrees of freedom, and n is the power law exponent. GPE is estimated assuming topography is Airy isostatically compensated in the Airy isostatic model, from the EGM96 geoid in the geoid model, and using seismic crustal thickness estimates (G. Laske and G. Masters, http://mahi.ucsd.edu/Gabi/sediment.html, 2000) in the seismic model.

able us to delineate the minimum size of crustal blocks within the collision zone. An important result in our quantification of the dynamics is the absolute value of vertically integrated deviatoric stresses over the 100-km-thick layer. The maximum deviatoric stress difference between Tibet and lower elevation regions is $\sim 3.2 \times 10^{12}$ N/m, which is 50% smaller than previously thought [*Molnar et al.*, 1993]. However, vertical deviatoric stresses $\overline{\tau}_{zz} = -(\overline{\tau}_{xx} + \overline{\tau}_{yy})$, of similar magnitude though opposite sign to the largest horizontal deviatoric stress $\overline{\tau}_{xx}$ or $\overline{\tau}_{yy}$, are incorporated in our calculations, whereas deviatoric stresses in previous calculations were implicitly defined with $\overline{\tau}_{zz}$ subtracted from $\overline{\tau}_{xx}$, $\overline{\tau}_{yy}$, and $\overline{\tau}_{zz}$, leaving $\overline{\tau}_{zz} = 0$.

Calculations from the published strength profile from *Kohlstedt et al.* [1995] and our vertically averaged deviatoric stress and effective viscosity estimates yields maximum values of 100-300 MPa of deviatoric stress in the seismogenic zone, consistent with rock mechanics experiments [*Sibson*, 1982; *Kohlstedt et al.*, 1995]. This result suggests that a significant portion of the strength of the lithosphere resides within the seismogenic portion of the crust [e.g., *Maggi et al.*, 2000].

Our results for a low effective vertically averaged viscosity for Tibet are in agreement with previous suggestions that the lower crust there might be weak or might contain partial melt [*Bird*, 1991; *Fielding et al.*, 1994; *Masek et al.*, 1994; *Nelson et al.*, 1996; *Owens and Zandt*, 1997; *Royden et al.*, 1997]. The correlation of low values of vertically averaged effective viscosity (n=1) with regions of thick continental crust (Plate 1a) also agrees with recent interpretation of gravity anomalies [*McKenzie and Fairhead*, 1997], indicating that continental lithosphere is not capable of supporting elastic stresses over geologic timescales at temperatures above ~350°C.

Appendix A

We find the minimization constraints for equations (2a) and (2b) by first using the product rule to rewrite equation (4):

$$I = \int_S \left[\overline{\tau}_{\alpha\beta}\overline{\tau}_{\alpha\beta} + (\overline{\tau}_{\gamma\gamma})^2\right] dS$$

$$- \int_S 2\frac{\partial \lambda_\alpha}{\partial x_\beta}\left[\delta_{\alpha\beta}\overline{\sigma}_{zz} + \overline{\tau}_{\alpha\beta} + \delta_{\alpha\beta}\overline{\tau}_{\gamma\gamma}\right] dS$$

$$+ \int_S 2\frac{\partial}{\partial x_\beta}\left(\lambda_\alpha\left[\delta_{\alpha\beta}\overline{\sigma}_{zz} + \overline{\tau}_{\alpha\beta} + \delta_{\alpha\beta}\overline{\tau}_{\gamma\gamma}\right]\right) dS \qquad \text{(A1)}$$

and then applying the divergence theorem to (A1), which yields

$$I = \int_S \left[\overline{\tau}_{\alpha\beta}\overline{\tau}_{\alpha\beta} + (\overline{\tau}_{\gamma\gamma})^2\right] dS$$

$$- \int_S 2\frac{\partial \lambda_\alpha}{\partial x_\beta}\left[\delta_{\alpha\beta}\overline{\sigma}_{zz} + \overline{\tau}_{\alpha\beta} + \delta_{\alpha\beta}\overline{\tau}_{\gamma\gamma}\right] dS$$

$$+ \int_{\partial S} 2\lambda_\alpha\left[\delta_{\alpha\beta}\overline{\sigma}_{zz} + \overline{\tau}_{\alpha\beta} + \delta_{\alpha\beta}\overline{\tau}_{\gamma\gamma}\right] n_\beta d\ell, \qquad \text{(A2)}$$

where ∂S is the boundary around S, $d\ell$ is the increment of the line length around ∂S, and (n_x, n_y) is the outward normal around ∂S. The symmetry of $\overline{\tau}_{\alpha\beta}$ and

Table 3. Goodness of Fit of Dynamic Velocity Fields for Different Power Law Rheologies and Methods of Estimating Gravitational Potential Energy to GPS Measurements[a]

n	Model	Total SSM	DoF	RMS Misfit
3	Airy isostatic	4110.4	664	2.488
5	Airy isostatic	5914.2	664	2.984
3	geoid	3684.7	664	2.356
5	geoid	3787.7	664	2.388
3	seismic	3859.7	664	2.411
5	seismic	4879.4	664	2.711

[a]SSM is the sum of squared misfit between the model and observed velocity components. Each squared misfit in the summation is weighted by the variance in observed velocity component. DoF is the number of degrees of freedom, which is equal to 2 times the number of velocity observations. RMS misfit is the square root of the quantity of the total weighted SSM divided by the number of degrees of freedom, and n is the assumed power law exponent. Models are the same as those described in Table 2.

$\delta_{\alpha\beta}$ allows (A2) to be written as

$$I = \int_s \left[\overline{\tau}_{\alpha\beta}\overline{\tau}_{\alpha\beta} + (\overline{\tau}_{\gamma\gamma})^2\right] dS$$

$$- \int_s \left(\frac{\partial\lambda_\alpha}{\partial x_\beta} + \frac{\partial\lambda_\beta}{\partial x_\alpha}\right) [\delta_{\alpha\beta}\overline{\sigma}_{zz} + \overline{\tau}_{\alpha\beta} + \delta_{\alpha\beta}\overline{\tau}_{\gamma\gamma}]\, dS$$

$$+ \int_{\partial S} 2\lambda_\alpha [\overline{\sigma}_{zz}n_\alpha + \overline{\tau}_{\alpha\beta}n_\beta + \overline{\tau}_{\gamma\gamma}n_\alpha]\, d\ell. \qquad \text{(A3)}$$

Using the variational principle [*Morse and Feshbach*, 1953] to minimize I in (A3) with respect to $\overline{\tau}_{\alpha\beta}$, we evaluate $\delta I\,(\tau_{\alpha\beta} + d\tau_{\alpha\beta}) = 0$ as $d\tau_{\alpha\beta} \to 0$:

$$I = \int_S \left[(\overline{\tau}_{\alpha\beta} + d\tau_{\alpha\beta})\,(\overline{\tau}_{\alpha\beta} + d\tau_{\alpha\beta}) + (\overline{\tau}_{\gamma\gamma} + d\tau_{\gamma\gamma})^2\right] dS$$

$$- \int_s \left(\frac{\partial\lambda_\alpha}{\partial x_\beta} + \frac{\partial\lambda_\beta}{\partial x_\alpha}\right)$$

$$[\delta_{\alpha\beta}\overline{\sigma}_{zz} + (\overline{\tau}_{\alpha\beta} + d\tau_{\alpha\beta}) + \delta_{\alpha\beta}\,(\overline{\tau}_{\gamma\gamma} + d\tau_{\gamma\gamma})]\, dS$$

$$+ \int_{\partial S} 2\lambda_\alpha\, [\overline{\sigma}_{zz}n_\alpha$$

$$+ (\overline{\tau}_{\alpha\beta} + d\tau_{\alpha\beta})\, n_\beta + (\overline{\tau}_{\gamma\gamma} + d\tau_{\gamma\gamma})\, n_\alpha]\, d\ell. \qquad \text{(A4)}$$

For the functional I to be a minimum only terms involving products with $d\tau_{\alpha\beta}$ are considered and thus

$$\delta I = \int_S \{[2\overline{\tau}_{\alpha\beta} + 2\overline{\tau}_{\gamma\gamma}$$

$$- \left(\frac{\partial\lambda_\alpha}{\partial x_\beta} + \frac{\partial\lambda_\beta}{\partial x_\alpha}\right) - 2\frac{\partial\lambda_\gamma}{\partial x_\gamma}\delta_{\alpha\beta}\Big]\, d\tau_{\alpha\beta}\Big\}\, dS$$

$$+ \int_{\partial S} ([2\lambda_\alpha n_\beta + 2\lambda_\gamma n_\gamma \delta_{\alpha\beta}]\, d\tau_{\alpha\beta})\, d\ell = 0. \qquad \text{(A5)}$$

In order for (A5) to hold true as $d\tau_{\alpha\beta} \to 0$ requires that

$$0 = [2\lambda_\alpha n_\beta + 2\lambda_\gamma n_\gamma \delta_{\alpha\beta}]$$

on ∂S from the third line of (A5) and

$$0 = 2\overline{\tau}_{\alpha\beta} + 2\overline{\tau}_{\gamma\gamma}\delta_{\alpha\beta} - \left(\frac{\partial\lambda_\alpha}{\partial x_\beta} + \frac{\partial\lambda_\beta}{\partial x_\alpha}\right) - 2\frac{\partial\lambda_\gamma}{\partial x_\gamma}\delta_{\alpha\beta}.$$

Therefore $\Lambda_i = (\lambda_\alpha, \lambda_\beta) = 0$ at all points on the boundary ∂S and

$$\overline{\tau}_{\alpha\beta} = \frac{1}{2}\left(\frac{\partial\lambda_\alpha}{\partial x_\beta} + \frac{\partial\lambda_\beta}{\partial x_\alpha}\right)$$

at all points inside S.

Appendix B

We construct a second functional that when minimized will ensure that equations (6) are satisfied:

$$J = \int_S \left[2\left(\overline{\tau}_{xx} + \frac{1}{3}\overline{\sigma}_{zz}\right)^2 + 2\left(\overline{\tau}_{xx} + \frac{1}{3}\overline{\sigma}_{zz}\right)\right.$$

$$\left.\left(\overline{\tau}_{yy} + \frac{1}{3}\overline{\sigma}_{zz}\right) + 2\left(\overline{\tau}_{yy} + \frac{1}{3}\overline{\sigma}_{zz}\right)^2 + 2\overline{\tau}_{xy}^2\right] dS, \qquad \text{(B1)}$$

where α and β have now been summed over x and y. Substituting (5) into (B1), we have

$$J = \int_S \left[2\left(\frac{\partial\lambda_x}{\partial x} + \frac{1}{3}\overline{\sigma}_{zz}\right)^2\right.$$

$$+2\left(\frac{\partial\lambda_x}{\partial x} + \frac{1}{3}\overline{\sigma}_{zz}\right)\left(\frac{\partial\lambda_y}{\partial y} + \frac{1}{3}\overline{\sigma}_{zz}\right)$$

$$\left.+2\left(\frac{\partial\lambda_y}{\partial y} + \frac{1}{3}\overline{\sigma}_{zz}\right)^2 + \frac{1}{2}\left(\frac{\partial\lambda_x}{\partial y} + \frac{\partial\lambda_y}{\partial x}\right)^2\right] dS. \qquad \text{(B2)}$$

Using the variational principle [*Morse and Feshbach*, 1953] with respect to changes in $\Lambda_i = (\lambda_x, \lambda_y)$, it can be shown that minimization of (B2) satisfies the force balance equations. For example, for changes ϵ_x in λ_x to $(\lambda_x + \epsilon_x)$, δJ can be written as

$$\delta J = \int_S \left[4\left(\frac{\partial\lambda_x}{\partial x} + \frac{1}{3}\overline{\sigma}_{zz}\right)\frac{\partial\epsilon_x}{\partial x}\right.$$

$$+2\left(\frac{\partial\lambda_y}{\partial y} + \frac{1}{3}\overline{\sigma}_{zz}\right)\frac{\partial\epsilon_x}{\partial x}$$

$$\left.+\left(\frac{\partial\lambda_x}{\partial y} + \frac{\partial\lambda_y}{\partial x}\right)\frac{\partial\epsilon_x}{\partial y}\right] dS = 0. \qquad \text{(B3)}$$

Then making use of the product rule and applying the divergence theorem and using $\epsilon_x = 0$ on ∂S, (B3) becomes

$$-\int_S \left[4\frac{\partial}{\partial x}\left(\frac{\partial\lambda_x}{\partial x} + \frac{1}{3}\overline{\sigma}_{zz}\right) + 2\frac{\partial}{\partial x}\left(\frac{\partial\lambda_y}{\partial y} + \frac{1}{3}\overline{\sigma}_{zz}\right)\right.$$

$$\left.+\frac{\partial}{\partial y}\left(\frac{\partial\lambda_x}{\partial y} + \frac{\partial\lambda_y}{\partial x}\right)\right]\epsilon_x dS = 0. \qquad \text{(B4)}$$

Equation (B4) requires that

$$\frac{\partial}{\partial x}\left(2\frac{\partial\lambda_x}{\partial x} + \frac{\partial\lambda_y}{\partial y}\right) + \frac{1}{2}\frac{\partial}{\partial y}\left(\frac{\partial\lambda_x}{\partial y} + \frac{\partial\lambda_y}{\partial x}\right) = -\frac{\partial\overline{\sigma}_{zz}}{\partial x}$$

which satisfies the first of the two equations in (6). Minimizing (B2) by applying the variational principle of changes in λ_y to $(\lambda_y + \epsilon_y)$ gives the second differential equation constraint

$$\frac{\partial}{\partial y}\left(2\frac{\partial \lambda_y}{\partial y}+\frac{\partial \lambda_x}{\partial x}\right)+\frac{1}{2}\frac{\partial}{\partial x}\left(\frac{\partial \lambda_x}{\partial y}+\frac{\partial \lambda_y}{\partial x}\right)=-\frac{\partial \overline{\sigma}_{zz}}{\partial y}.$$

The minimization of (7) therefore provides a solution to (2a), (2b), and (6) for the minimum vertically averaged deviatoric stress resulting from GPE differences in the lithosphere.

Appendix C

We will show that with a defined distribution of viscosity, body forces, and velocity boundary conditions the minimization of

$$\Theta(\nu)=\int\int_s [D-\nu_\alpha f_\alpha]\,dxdy \tag{C1}$$

provides a solution to the force balance equations, where f_α is the body force term associated with the gravitational potential ($f_\alpha = \partial\overline{\sigma}_{zz}/\partial x_\alpha$), ν_α is the velocity, and D is the dissipation potential. The dissipation potential depends on the B value, the strain rates, and the power law exponent n,

$$D=\frac{n}{n+1}B\left(\dot{\varepsilon}_{\alpha\beta}\dot{\varepsilon}_{\alpha\beta}+\dot{\varepsilon}_{\gamma\gamma}\dot{\varepsilon}_{\gamma\gamma}\right)^{\frac{n+1}{2n}}. \tag{C2}$$

Now consider a small perturbation to $\Theta(\nu)$ of $\Theta(\nu+\epsilon u)$. Then for any value of u, a minimum of $\Theta(\nu)$ will occur when $d/d\epsilon\left[\Theta(\nu+\epsilon u)\right]|_{\epsilon=0}=0$. Now write $dD/d\epsilon$ using the chain rule and evaluate the derivatives

$$\frac{dD}{d\epsilon}=\frac{\partial D}{\partial \dot{\varepsilon}_{\alpha\beta}}$$

$$\frac{d}{d\epsilon}\left\{\frac{1}{2}\left(\frac{\partial \nu_\alpha}{\partial x_\beta}+\frac{\partial \nu_\beta}{\partial x_\alpha}\right)+\epsilon\frac{1}{2}\left(\frac{\partial u_\alpha}{\partial x_\beta}+\frac{\partial u_\beta}{\partial u_\alpha}\right)\right\}. \tag{C3}$$

Evaluating (C3) we have

$$\frac{dD}{d\epsilon}=\overline{\tau}_{\alpha\beta}\frac{1}{2}\left(\frac{\partial u_\alpha}{\partial x_\beta}+\frac{\partial u_\beta}{\partial x_\alpha}\right), \tag{C4}$$

where $\overline{\tau}_{\alpha\beta}$ is the general stress when $\epsilon\neq 0$. In order to simplify, stress $\overline{\tau}_{\alpha\beta}$ and those below represent the two-dimensional case where vertical deviatoric stress $\overline{\tau}_{zz}$ is defined to be zero, instead of using the constraint $\overline{\tau}_{xx}+\overline{\tau}_{yy}+\overline{\tau}_{zz}=0$ to define $\overline{\tau}_{zz}$ (i.e., $\overline{\tau}_{zz}=0$, and $\overline{\tau}_{ij}=\overline{\sigma}_{ij}-\overline{\sigma}_{zz}\delta_{ij}$, rather than $\overline{\tau}_{xx}+\overline{\tau}_{yy}+\overline{\tau}_{zz}=0$ and $\overline{\tau}_{ij}=\overline{\sigma}_{ij}-\frac{1}{3}(\overline{\sigma}_{xx}+\overline{\sigma}_{yy}+\overline{\sigma}_{zz})\delta_{ij}$). Using the symmetry of $\overline{\tau}_{\alpha\beta}=\overline{\tau}_{\beta\alpha}$, (C4) can be written as

$$\frac{dD}{d\epsilon}=\frac{1}{2}\overline{\tau}_{\alpha\beta}\frac{\partial u_\alpha}{\partial x_\beta}+\frac{1}{2}\overline{\tau}_{\beta\alpha}\frac{\partial u_\alpha}{\partial x_\beta}=\overline{\tau}_{\alpha\beta}\frac{\partial u_\alpha}{\partial x_\beta}. \tag{C5}$$

Finally, recall that

$$\frac{d}{d\epsilon}\left(\nu_\alpha f_\alpha+\epsilon u_\alpha f_\alpha\right)=u_\alpha f_\alpha. \tag{C6}$$

Now consider a particular value of u at $\epsilon=0$ where stress is at a minimum

$$\frac{d\Theta}{d\epsilon}|_{\epsilon=0}=\int\int_S\left[\frac{dD}{d\epsilon}-\frac{d}{d\epsilon}(\nu_\alpha f_\alpha)\right]dxdy=0 \tag{C7}$$

substituting (C5 and C6) into (C7), it becomes

$$\frac{d\Theta}{d\epsilon}|_{\epsilon=0}=\int\int_S\left[\overline{\tau}_{\alpha\beta}\frac{\partial u_\alpha}{\partial x_\beta}-u_\alpha f_\alpha\right]dxdy=0. \tag{C8}$$

Using the product rule, the first term included within the integrals in (C8) can be written as

$$\frac{\partial}{\partial x_\beta}(\overline{\tau}_{\alpha\beta}u_\alpha)-\frac{\partial \overline{\tau}_{\alpha\beta}}{\partial x_\beta}u_\alpha=\overline{\tau}_{\alpha\beta}\frac{\partial u_\alpha}{\partial x_\beta}. \tag{C9}$$

Substituting (C9) into (C8) yields

$$\frac{d\Theta}{d\epsilon}|_{\epsilon=0}=\int\int_S\frac{\partial}{\partial x_\beta}(\overline{\tau}_{\alpha\beta}u_\alpha)\,dxdy$$

$$-\int\int_S\left(\frac{\partial \overline{\tau}_{\alpha\beta}}{\partial x_\beta}u_\alpha+u_\alpha f_\alpha\right)dxdy=0. \tag{C10}$$

Applying the divergence theorem to the first term on the right hand side of (C10) yields

$$\frac{d\Theta}{d\epsilon}|_{\epsilon=0}=\int_{\partial S}\overline{\tau}_{\alpha\beta}u_\alpha n_\beta d\ell$$

$$-\int\int_S u_\alpha\left(\frac{\partial \overline{\tau}_{\alpha\beta}}{\partial x_\beta}+f_\alpha\right)dxdy=0, \tag{C11}$$

where ∂S is the boundary around S, $d\ell$ is the increment of the line length around ∂S. For (C11) to be at a minimum, $d\Theta/d\epsilon=0$ for any function u. In particular, for u such that $u=0$ on ∂S, which requires that $\int_{\partial S}u_\alpha\overline{\tau}_{\alpha\beta}n_\beta d\ell=0$; therefore (C11) becomes

$$\frac{d\Theta}{d\epsilon}|_{\epsilon=0}=\int\int_S u_\alpha\left(\frac{\partial \overline{\tau}_{\alpha\beta}}{\partial x_\beta}+f_\alpha\right)dxdy=0. \tag{C12}$$

This set of such functions u in (C12) contains functions that are arbitrarily close to any function in the set of all possible u (including those with $u\neq 0$ on ∂S). A consequence for this is that

$$\frac{\partial \overline{\tau}_{\alpha\beta}}{\partial x_\beta}+f_\alpha=0 \tag{C13}$$

everywhere inside S, which is the force balance equations (2a) and (2b) when the two-dimensional deviatoric stresses (with $\overline{\tau}_{zz}=0$) are converted to the three-dimensional deviatoric stresses (with $\overline{\tau}_{zz}=-(\overline{\tau}_{xx}+\overline{\tau}_{yy})$) used everywhere in the paper, apart from here and in Appendix D. Therefore the minimization of (C13) provides a solution to the force balance equations and is appropriate to use to perform forward modeling, given that we have properly defined D (equation (14)) and given that the distribution of $f_\alpha=\partial\overline{\sigma}_{zz}/\partial x_\alpha$ is known.

Appendix D

The minimization of (13) involves the minimization of (15):

$$\Theta = \int\int_S [D + \dot{\varepsilon}_{\gamma\gamma}\overline{\sigma}_{zz}]\,dxdy - \int_{\partial S} \nu_\alpha \overline{\sigma}_{zz} n_\alpha d\ell \quad \text{(D1)}$$

The second term in (D1) contains the plate motion boundary conditions which is not influenced by the minimization of (D1); only the first integral is influenced in the minimization. The depth averaged two-dimensional deviatoric stresses $\overline{\tau}_{\alpha\beta} = (1/h)\int_0^h \tau_{\alpha\beta} dz$ are given by $\overline{\tau}_{\alpha\beta} = \partial D/\partial\dot{\varepsilon}_{\alpha\beta}$. Now assume some initial estimate of the strain rate field, $\dot{\varepsilon}^0_{\alpha\beta}$, that has associated deviatoric stresses $\overline{\tau}^0_{\alpha\beta} = \partial D/\partial\dot{\varepsilon}_{\alpha\beta}\,|_{\dot{\varepsilon}=\dot{\varepsilon}^0}$, where $\dot{\varepsilon}$ denotes the strain rate tensor, and let $\nu^0_{\alpha\beta\gamma\delta} = \partial^2 D/\partial\dot{\varepsilon}_{\alpha\beta}\partial\dot{\varepsilon}_{\gamma\delta}\,|_{\dot{\varepsilon}=\dot{\varepsilon}^0}$ and D_0 be the value of D when $\dot{\varepsilon} = \dot{\varepsilon}^0$. Using the above expressions and expanding the first integral in (D1) to second order in $\dot{\varepsilon} - \dot{\varepsilon}^0$ using a Taylor series expansion of D with respect to $\dot{\varepsilon}$ yields

$$\int\int_S [D_0 + \overline{\tau}^0_{\alpha\beta}\left(\dot{\varepsilon}_{\alpha\beta} - \dot{\varepsilon}^0_{\alpha\beta}\right)$$

$$+\frac{1}{2}\nu^0_{\alpha\beta\gamma\delta}\left(\dot{\varepsilon}_{\alpha\beta} - \dot{\varepsilon}^0_{\alpha\beta}\right)\left(\dot{\varepsilon}_{\gamma\delta} - \dot{\varepsilon}^0_{\gamma\delta}\right)$$

$$+\dot{\varepsilon}_{\gamma\gamma}\overline{\sigma}_{zz}]\,dxdy. \quad \text{(D2)}$$

With some initial strain rate values, $\dot{\varepsilon}^0_{\alpha\beta}$, (D2) can be minimized to determine a forward modeled strain rate field, velocity field, and deviatoric stress field for a given power law rheology. The initial estimate of $\dot{\varepsilon}^0_{\alpha\beta}$ is determined by dividing each element of the deviatoric stress tensor field calculated in section 3 by the magnitude of viscosity determined in section 4. The B value distributions used for a given power law are those determined in section 4, and the body force distribution used is that calculated in section 2. We then determine $\dot{\varepsilon}_{\alpha\beta}$ by minimization of (D2) with respect to velocity field and strain rate using a finite element approach with the kinematic velocity boundary conditions from *Holt et al.* [2000a, 2000b] determined from Quaternary fault slip data and GPS velocities imposed along the boundary of our grid. The resulting values of $\dot{\varepsilon}_{\alpha\beta}$ are then input as the new initial estimate $\dot{\varepsilon}^0_{\alpha\beta}$, and we continue to iterate about $\dot{\varepsilon}^0_{\alpha\beta}$ until the solution converges, which, for the values of n=3 and n=5, occurred after three iterations.

Acknowledgments. We thank Dan Davis and Troy Rasbury for fruitful discussions and Dan McKenzie, Philip England, Peter Molnar, Jean Chery, Barry Parsons, Leigh Royden, and Xavier Le Pichon for helpful comments and reviews on the manuscript. We thank Bingming Shen-Tu for help in producing some of the figures. We are grateful to B. Hager, B. Ambrosius, Bob King, and W. Zhu for providing GPS data and G. Laske and G. Masters for providing the crustal thickness data. Maps were prepared using GMT version 3.0 by P. Wessel and W.F. Smith. This work was supported by NSF grants EAR-9268872 and EAR-9909621 to W.E.H. A.J.H.'s contribution has been supported by the Marsden Fund administered by the Royal Society of New Zealand. Cambridge Earth Sciences contribution 5499.

References

Abdrakhmatov, K., et al., Relatively recent construction of the Tien Shan inferred from GPS measurements of present-day crustal deformation rates, *Nature, 384*, 450-453, 1996.

Armijo, R., P. Tapponnier, J. L. Mercier, and Hon T.-L., Quaternary extension in southern Tibet: Field observations and tectonic implications, *J. Geophys. Res., 91*, 13,803-13,872, 1986.

Artyushkov, E. V., Stresses in the lithosphere caused by crustal thickness inhomogeneities, *J. Geophys. Res., 78*, 7675-7690, 1973.

Avouac, J.P., and P. Tapponnier, Kinematic model of active deformation in central Asia, *Geophys. Res. Lett., 20*, 895-898, 1993.

Bendick, R., R. Bilham, J. Freymueller, K. Larson, and G. H. Yin, Geodetic evidence for a low slip rate in the Altyn Tagh fault system, *Nature, 404*, 69-72, 2000.

Bird, P., Lateral extrusion of lower crust from under high topography, in the isostatic limit, *J. Geophys. Res., 96*, 10,275-10,286, 1991.

Bird, P., and K. Piper, Plane-stress finite-element models of tectonic flow in southern California, *Phys. Earth Planet. Inter., 21*, 158-175, 1980.

Bird, R.B., New variational principle for incompressible non-Newtonian flow, *Phys. Fluids, 3*, 539-541, 1960.

Brandon, C., and B. Romanowicz, A no-lid zone in the central Chang-Thang platform of Tibet: Evidence from pure path phase velocity measurements of long period rayleigh waves, *J. Geophys. Res., 91*, 6547-6564, 1986.

Brudy, M., M.D. Zoback, K. Fuchs, F. Rummel, and J. Baumgartner, Estimation of the complete stress tensor to 8 km depth in the KTB scientific drill holes: Implication for crustal strength, *J. Geophys. Res., 102*, 18,453-18,475, 1997.

Burchfiel, B.C., and L.H. Royden, Tectonics of Asia 50 years after the death of Argand, Emile, *Eclogae Geol. Helv., 84*, 599-629, 1991.

Calais, E., O. Lesne, J. Dechere, V. San'kov, A. Lukhnev, A. Miroshnitchenko, V. Buddo, K. Levi, V. Zaultzky, and Y. Bashkuev, Crustal deformation in the Baikal rift from GPS measurements, *Geophys. Res. Lett., 25*, 4003-4006, 1998.

Chen, Z., B.C. Burchfiel, Y. Liu, R.W. King, L.H. Royden, W. Tang, E. Wang, J. Zhao, and X. Zhang, Global Positioning System measurements from eastern Tibet and their implications for India/Eurasia intercontinental deformation, *J. Geophys. Res., 105*, 16,215-16,228, 2000.

Cobbold, P.R., and P. Davy, Indentation tectonics in nature and experiment, 2, Central Asia, *Bull. Geol. Inst. Uppsala, 14*, 143-162, 1988.

Coblentz, D. D., R. M. Richardson, and M. Sandiford, On the gravitational potential of the Earth's lithosphere, *Tectonics, 13*, 929-945, 1994.

Dalmayrac, B., and P. Molnar, Parallel thrust and normal faulting in Peru and constraints on the state of stress, *Earth Planet. Sci. Lett., 55*, 473-481, 1981.

deBoor, C., *A Practical Guide to Splines*, Springer-Verlag, New York, 1978.

DeMets, C., R. G. Gordon, D. F. Argus, and S. Stein, Effects of recent revisions to the geomagnetic reversal time scale on estimates of current plate motions, *Geophys. Res. Lett., 21*, 2191-2194, 1994.

England, P., and G. Houseman, Finite strain calculations of continental deformation, 2, Comparison with the India-Asia collision zone, *J. Geophys. Res., 91*, 3664-3676, 1986.

England, P., and D. P. McKenzie, A thin viscous sheet model for continental deformation, *Geophys. J. R. Astron. Soc., 70*, 295-321, 1982.

England, P., and P. Molnar, The field of crustal velocity in Asia calculated from Quaternary rates of slip on faults, *Geophys. J. Int., 130*, 551-582, 1997a.

England, P. C., and P. Molnar, Active deformation of Asia: From kinematics to dynamics, *Science, 278*, 647-650, 1997b.

Fielding, E., B. Isacks, M. Barazangi, and C. Duncan, How flat is Tibet?, *Geology, 22*, 162-167, 1994.

Fleitout, L., and C. Froidevaux, Tectonics and topography for a lithosphere containing density heterogeneities, *Tectonics, 1*, 21-56, 1982.

Flesch, L.M., W.E. Holt, A.J. Haines, and B. Shen-Tu, Dynamics of the Pacific-North American plate boundary in the western United States, *Science, 287*, 834-836, 2000.

Frank, F.C., Plate tectonics, the analogy with glacier flow, and isostasy, in *Flow and Fracture of Rocks, Geophys. Monogr. Ser.*, vol. 16, edited by H.C. Heard et al., pp. 285-292, AGU, Washington, D. C., 1972.

Fung, Y.C., *Foundations of solid mechanics*, Prentice-Hall, Old Tappan, N. J., 1965.

Hager, B.H., R.W. Clayton, M.A. Richards, R.P. Comer, and A.M. Dziewonski, Lower mantle heterogeneity, dynamic topography and the geoid, *Nature, 331*, 541-545, 1985.

Haines, A. J., Calculating velocity fields across plate boundaries from observed shear rates, *Geophys. J. R. Astron. Soc., 68*, 203-209, 1982.

Haines, A. J., and W. E. Holt, A procedure for obtaining the complete horizontal motions within zones of distributed deformation from the inversion of strain rate data, *J. Geophys. Res., 98*, 12,057-12,082, 1993.

Haines, A. J., J. A. Jackson, W. E. Holt, and D. C. Agnew, Representing distributed deformation by continuous velocity fields, *Sci. Rep. 98/5*, Inst. of Geol. and Nucl. Sci., Wellington, New Zealand, 1998.

Heki, K., S. Miyazaki, H. Takahashi, M. Kasahara, F. Kimata, S. Miura, N. F. Vasilenko, A. Ivashchenko, and K. D. An, The Amurian plate motion and current plate kinematics in eastern Asia, *J. Geophys. Res., 104*, 29,147-29,155, 1999.

Hildebrand, F.B., Methods of Applied Mathematics, pp. 134-139, Prentice-Hall, Old Tappen, N. J., 1952.

Holt, W.E., J.F. Ni, T.C. Wallace, and A.J. Haines, The active tectonics of the eastern Himalayan syntasis and surrounding regions, *J. Geophys. Res., 96*, 14,595-14,632, 1991.

Holt, W. E., M. Li, and A. J. Haines, Earthquake strain rates and instantaneous relative motion within central and east Asia, *Geophys. J. Int., 122*, 569-593, 1995.

Holt, W. E., B. Shen-Tu, A. J. Haines, and J. Jackson, On the determination of self-consistent strain rate fields within zones of distributed continental deformation, in *The History and Dynamics of Plate Motions, Geophys. Monogr. Ser.*, vol. 121, edited by M.A. Richards, R. Gordon, and R.D. Van der Hilst, pp. 113-141 AGU, Washington, D. C., 2000a.

Holt, W. E., N. Chamot-Rooke, X. Le Pichon, and A. J. Haines, The velocity field in Asia inferred from Quaternary fault slip rates and GPS observations, *J. Geophys. Res., 105*, 19,185-19,209, 2000b.

Houseman, G., and P. England, Crustal thickening versus lateral expulsion in the Indian-Asian continental collision, *J. Geophys. Res., 98*, 12,233-12,249, 1993.

Jin, Y., M.K. McNutt, and Y. Zhu, Evidence from gravity and topography data for folding of Tibet, *Nature, 371*, 669-674, 1994.

Jones, C. H., J. R. Unruh, and L. J. Sonder, The role of gravitational potential energy in active deformation in the southwestern United States, *Nature, 381*, 37-41, 1996.

Kanamori, H., and D.L. Anderson, Theoretical Basis of some empirical relationship in seismology, *Bull. Seismol. Soc. Am.*, 65, 1073-1095, 1975.

Kohlstedt, D.L., B. Evens, and S.J. Mackwell, Strength of the lithosphere: Constraints imposed by laboratory experiments, *J. Geophys. Res., 100*, 17,587-17,601, 1995.

Kosarev, G., R. Kind, S.V. Sobolev, X. Yuan, W. Hanka, and S. Oreshin, Seismic evidence for a detached Indian lithospheric mantle beneath Tibet, *Science, 283*, 1306-1309, 1999.

Kronenberg, A.K., and J. Tullis, Flow strengths of quartz aggregates: Grain size and pressure effects due to hydrolytic weakening, *J. Geophys. Res., 89*, 4281-4297, 1984.

Larson, K. M., R. Burgmann, R. Bilham, and J. T. Freymueller, Kinematics of the India-Eurasia collision zone from GPS measurements, *J. Geophys. Res., 104*, 1077-1093, 1999.

Luan, F., and M.S. Paterson, Preparation and deformation of synthetic aggregates of quartz, *J. Geophys. Res., 97*, 301-320, 1992.

Maggi, A., J.A. Jackson, D. McKenzie, and K. Priestley, Earthquake focal depths, effective elastic thickness, and the strength of the continental lithosphere, *Geology, 28*, 495-498, 2000.

Masek, J. G., B. L. Isacks, and E. J. Fielding, Rift flank uplift in Tibet: Evidence for a viscous lower crust, *Tectonics, 13*, 659-667, 1994.

McKenzie, D., Active tectonics of Mediterranean region, *Geophys. J. R. Astron. Soc., 30*, 109-185, 1972.

McKenzie, D., and D. Fairhead, Estimates of the effective elastic thickness of the continental lithosphere from Bouguer and free air gravity anomalies, *J. Geophys. Res., 102*, 27,523-27,552, 1997.

McNamara, D. E., W. R. Walter, T. J. Owens, and C. J. Ammon, Upper mantle velocity structure beneath the Tibetan Plateau from *Pn* travel time tomography, *J. Geophys. Res., 102*, 493-505, 1997.

Molnar, P., Continental tectonics in the aftermath of plate tectonics, *Nature, 335*, 131-137, 1988.

Molnar, P., Brace-Goetze strength profiles, the partitioning of strike-slip and thrust faulting at zones of oblique convergence, and the stress-heat flow paradox of the San Andreas fault, in *Fault Mechanics and Transport Properties of Rocks, Int. Geophys. Rev.*, vol. 51, edited by B. Evans and T-f. Wong, pp. 435-459, Acedemic, San Diego, Calif., 1992.

Molnar, P., and Deng Q., Faulting associated with large earthquakes and the average rate of deformation in central and eastern Asia, *J. Geophys. Res., 89*, 6203-6228, 1984.

Molnar, P., and J. M. Gipson, A bound on the rheology of continental lithosphere using very long baseline interferometry: The velocity of south China with respect to Eurasia, *J. Geophys. Res., 101*, 545-553, 1996.

Molnar, P., and H. Lyon-Caen, Some simple physical aspects of the support, structure, and evolution of mountain belts, *Spec. Pap. Geol. Soc. Am., 218*, 179-207, 1988.

Molnar, P., and H. Lyon-Caen, Fault plane solutions of earthquakes and active tectonics of the northern and eastern parts of the Tibetan Plateau, *Geohpys. J. Int., 99*, 123-153, 1989.

Molnar, P., and P. Tapponnier, Cenozoic tectonics of Asia:

Effects of a continental collision, *Science, 189*, 419-425, 1975.

Molnar, P., P. England, and J. Martinod, Mantle dynamics, uplift of the Tibetian Plateau, and the Indian monsoon, *Rev. Geophys., 31*, 357-396, 1993.

Morse, P.M., and H. Feshbach, *Methods of Theoretical Physics*, pp. 257-347, McGraw-Hill, New York, 1953.

Nelson, K. D., et al., Partially molten middle crust beneath southern Tibet: Synthesis of Project INDEPTH results, *Science, 274*, 1684-1688, 1996.

Nelson, M.R., R. McCaffrey, and P. Molnar, Source parameters for 11 earthquakes in the Tien Shan, Central Asia, determined by *P* and *SH* waveform inversion, *J. Geophys. Res., 92*, 12,629-12,648, 1987.

Owens, T. J., and G. Zandt, Implications of crustal property variations for models of Tibetan Plateau evolution, *Nature, 387*, 37-43, 1997.

Peltzer, G., and F. Saucier, Present-day kinematics of Asia derived from geologic fault rates, *J. Geophys. Res., 101*, 27,943-27,956, 1996.

Peltzer, G., and P. Tapponnier, Formation and evolution of strike-slip faults, rifts, and basins during the India-Asia collision: An experimental approach, *J. Geophys. Res., 93*, 15,085-15,117, 1988.

Rogers, A. J., and S. Y. Schwartz, Lithospheric structure of the Qiangtang Terrane, northern Tibetan Plateau, from complete regional waveform modeling: Evidence for partial melt, *J. Geophys. Res., 103*, 7137-7152, 1998.

Royden, L. H., B. Clark Burchfiel, R. W. King, E. Wang, Z. Chen, F. Shen, and Y. Liu, Surface deformation and lower crustal flow in eastern Tibet, *Science, 276*, 788-790, 1997.

Sheehan, A.F., and S.C. Solomon, Joint inversion of shear wave travel time residuals and geoid and depth anomalies for long-wavelength variations in upper Mantle temperature and composition along the Mid-Atlantic Ridge, *J. Geophys. Res., 96*, 19,981-20,009, 1991.

Shen, Z.-K., C. Zhao, A. Yin, Y. Li, D. D. Jackson, P. Fang, and D. Dong, Contemporary crustal deformation in east Asia constrained by Global Positioning System measurements, *J. Geophys. Res., 105*, 5721-5734, 2000.

Sibson, R.H., Fault zone models, heat flow, and the depth distribution of earthquakes in the continental crust of the United States, *Bull. Seismol. Soc. Am., 72*, 151-163, 1982.

Silver, P. G., Seismic anisotropy beneath the continents, *Anu. Rev. Earth Planet. Sci., 24*, 385-432, 1996.

Simons, W. M. F., B. A. C. Ambrosius, R. Noomen, D. Angermann, P. Wilson, M. Becker, E. Reinhard, A. Walpersdorf, and C. Vigny, Observing plate motions in SE Asia: Geodetic results of the GEODYSSEA project, *Geophys. Res. Lett., 26*, 2081-2084, 1999.

Sonder, L. J., and P. C. England, Vertical averages of rheology of the continental lithosphere, *Earth Planet. Sci. Lett., 77*, 81-90, 1986.

Tapponnier, P., and P. Molnar, Slip-line field-theory and large scale continental tectonics, *Nature, 264*, 319-324, 1976.

Tapponnier, P., G. Peltzer, A.Y. Le Dain, R. Armijo, and P. Cobbold, Propagating extrusion tectonics in Asia: new insights from simple experiments with plasticine, *Geology, 10*, 611-616, 1982.

Vilotte, J. P., M. Daignieres, and R. Madariaga, Numerical modeling of intraplate deformation: Simple mechanical models of continental collision, *J. Geophys. Res., 87*, 19,709-10,728, 1982.

Wilson, P., et al., Study provides data on active plate tectonics in southeast Asia region, *Eos Trans. AGU, 79*, 545, 548-549, 1998.

Wittlinger, G., P. Tapponnier, G. Poupinet, J. Mei, S. Danian, G. Herquel, and F. Masson, Tomographic evidence for localized lithospheric shear along the Altyn Tagh fault, *Science, 282*, 74-76, 1998.

Yu, S.-B, L.-C Kuo, R.S. Punongbayan, and E.G. Ramos, GPS observation of crustal deformation in the Taiwan-Luzon, *Geophys. Res. Lett., 26*, 923-926, 1999.

Zhu, W. et al., Crustal motion of chinese mainland monitored by GPS, *Sci. China, Ser. D, 42*, 394-400, 2000.

L.M. Flesch and W.E. Holt, Department of Geosciences, SUNY-Stony Brook, Stony Brook, NY 11794-2100. (flesch@horizon.ess.sunysb.edu; wholt@horizon.ess.sunysb.edu)

A.J. Haines, Bullard Laboratories, University of Cambridge, Cambridge CB3 OEZ, England, U.K. (haines@esc.cam.ac.uk)

(Received September 22, 1999; revised March 24, 2001; accepted March 24, 2001.)